

Review

A Brief Review on the Latest Developments on Pharmaceutical Compound Degradation Using g-C₃N₄-Based Composite Catalysts

Subhadeep Biswas¹ and Anjali Pal^{2,*} 

¹ Civil Engineering Department, Swami Vivekananda Institute of Science and Technology, Kolkata 700145, West Bengal, India; sdeep0819@gmail.com

² Civil Engineering Department, Indian Institute of Technology Kharagpur, Kharagpur 721302, West Bengal, India

* Correspondence: anjalipal@civil.iitkgp.ac.in; Tel.: +91-3222-281920; Fax: +91-3222-282254

Abstract: Pharmaceutical compounds (PCs) are one of the most notable water pollutants of the current age with severe impacts on the ecosystem. Hence, scientists and engineers are continuously working on developing different materials and technologies to eradicate PCs from aqueous media. Among various new-age materials, graphitic carbon nitride (g-C₃N₄) is one of the wonder substances with excellent catalytic property. The current review article describes the latest trend in the application of g-C₃N₄-based catalyst materials towards the degradation of various kinds of drugs and pharmaceutical products present in wastewater. The synthesis procedure of different g-C₃N₄-based catalysts is covered in brief, and this is followed by different PCs degraded as described by different workers. The applicability of these novel catalysts in the real field has been highlighted along with different optimization techniques in practice. Different techniques often explored to characterize the g-C₃N₄-based materials are also described. Finally, existing challenges in this field along with future perspectives are presented before concluding the article.

Keywords: pharmaceutical compounds; g-C₃N₄; catalyst; wastewater; treatment



Citation: Biswas, S.; Pal, A. A Brief Review on the Latest Developments on Pharmaceutical Compound Degradation Using g-C₃N₄-Based Composite Catalysts. *Catalysts* **2023**, *13*, 925. <https://doi.org/10.3390/catal13060925>

Academic Editors: Weilong Shi, Feng Guo, Xue Lin and Yuanzhi Hong

Received: 15 April 2023

Revised: 15 May 2023

Accepted: 17 May 2023

Published: 24 May 2023



Copyright: © 2023 by the authors. Licensee MDPI, Basel, Switzerland. This article is an open access article distributed under the terms and conditions of the Creative Commons Attribution (CC BY) license (<https://creativecommons.org/licenses/by/4.0/>).

1. Introduction

Emerging contaminants are the most alarming water pollutants of the present era. Pharmaceutical compounds (PCs) have become one of the notable classes of emerging water pollutants [1]. These compounds have been detected in various concentration ranges (ng/L to µg/L) in natural water bodies. These compounds are reported to be present in natural water bodies, such as Taihu Lake in China and Mississippi River in the USA [2]. Moreover, an estimation has shown that till now at least 3000 species of PCs have been detected in water and wastewater [3]. Among various categories of drug compounds, nonsteroidal anti-inflammatory drugs and sulfonamides are often used for the treatment of various categories of diseases. However, the long-term existence of these compounds in natural water bodies leads to the chronic poisoning of the aquatic lives. Various drugs have been marked by several environmental agencies for their toxic effects. Naproxen (NPX), a drug often used to treat menstrual cramps, has been enlisted by US EPA as Class I in Current Contaminant Candidate List. Diclofenac (DC), a commonly used painkiller, is well known for its bioaccumulation and toxic characteristics. Evidence shows that it causes hemodynamic changes and thyroid tumor in humans [4].

Moreover, due to the COVID-19 pandemic, their concentration has increased drastically in the environmental matrices. Morales-Paredes et al. [5] in their recent review article mentioned the abnormal increase in the concentration range of these compounds in natural water and wastewater. Among several antiviral drugs used during the COVID-19 times, azithromycin and chloroquine are some of the most commonly used PCs. The concentration

of azithromycin drug is increased by 217 times in comparison to the normal concentration (WWTP-river-estuary at Wuhan, China). Due to various toxic effects, its removal from water streams is of utmost importance to environmental scientists and engineers. Conventional biological water treatment processes, adsorption, and coagulation are not feasible for the ultimate destruction of these recalcitrant compounds in aqueous media.

Eradication of organic compounds is possible through photocatalytic reaction, which undoubtedly is one of the green waste management options. In this regard, it may be noted that $g\text{-C}_3\text{N}_4$ is a prominent photocatalyst of the new age. It provides an attractive option to the research community for synthesizing noble metal-free efficient semiconductor-based photocatalysts. It possesses several distinguishing features such as higher thermal and chemical stability, due to the presence of strong covalent bonds between the C and N atoms in the conjugated $g\text{-C}_3\text{N}_4$ framework in it. It is easily prepared and nontoxic in nature [6]. However, the high probability of charge recombination, small surface area, and low reusability are some of the major hindrances behind its large-scale application [7]. Often these hurdles are minimized by means of doping [8], co-doping, co-polymerization via hybridization, exfoliation [9,10], formation of heterojunction structures [11], etc. A significant amount of research work has been performed by scientists all over the globe in recent times regarding the modification of $g\text{-C}_3\text{N}_4$ and its application for the treatment of PC-bearing wastewater. The current review article aims to focus on the latest trends in the applications of $g\text{-C}_3\text{N}_4$ -based composite photocatalysts towards PC wastewater remediation. Firstly, different types of $g\text{-C}_3\text{N}_4$ -based catalysts and their novel synthesis procedures are discussed. After that, various types of $g\text{-C}_3\text{N}_4$ -based catalysts applied for PC wastewater treatment in recent times have been elaborated. The next two sections deal with the optimization and applicability of different $g\text{-C}_3\text{N}_4$ -based catalysts for real wastewater treatment. Several characterization procedures often followed to get better insight into the removal process are then mentioned. The last section mentions the current challenges and future perspectives. This is followed by the concluding remarks. Almost all the papers discussed here have been published within the last five years.

2. Synthesis of Different Types of $g\text{-C}_3\text{N}_4$ -Based Catalysts for PC Degradation

Different types of $g\text{-C}_3\text{N}_4$ -based catalysts have been reported in the literature regarding the degradation of PCs. In the current section of this article, three categories have been selected for distinguishing $g\text{-C}_3\text{N}_4$ -based catalysts in respect of preparation technique. Firstly, they have been differentiated on the basis of the precursor material used for the production of $g\text{-C}_3\text{N}_4$. Different starting materials, such as melamine, urea, and dicyanamide, have been reported in the literature for the preparation of $g\text{-C}_3\text{N}_4$. Therefore, the first categorization describes the synthesis procedure of different novel catalysts from different precursor materials.

Moreover, it has been stated in the previous section that in comparison to the bare $g\text{-C}_3\text{N}_4$, composite formation with other materials and doping improved the catalytic efficiency. Hence, the next two subsections deal with the preparation procedure of several $g\text{-C}_3\text{N}_4$ composite and doped catalysts. As the classification is based on different criteria, a particular catalyst may satisfy more than one principle.

2.1. Various Precursors for Preparing $g\text{-C}_3\text{N}_4$

In $g\text{-C}_3\text{N}_4$, nitrogen is placed in a framework of graphite with a p-conjugated system and the distance between the two layers is 0.326 nm. $g\text{-C}_3\text{N}_4$ is often produced from a precursor material such as urea. Upon condensation of urea molecules, NH_3 and CO_2 gases are produced, which ultimately helps in the production of porous $g\text{-C}_3\text{N}_4$. However, in comparison to pure $g\text{-C}_3\text{N}_4$ catalysts, doped materials are often preferred by the research community for their improved photocatalytic features. Due to the doping with Na or K, the potentials of the valence band and conduction band for absorbing visible light are enhanced, which ultimately leads to increased photocatalytic activity. Guo et al. [12] reported the preparation of $g\text{-C}_3\text{N}_4$ nanosheets from urea. Briefly, urea was placed inside

an alumina crucible and heated to 550 °C for 3 h at the rate of 5 °C/min. The obtained yellow powder was heated for the second time in a muffle furnace at 52 °C to complete the thermal polymerization reaction and g-C₃N₄ nanosheets were produced.

Many studies reported the synthesis of g-C₃N₄ from melamine as the precursor. Chi et al. [13] prepared a g-C₃N₄-based catalyst from melamine. Guo et al. [14] also prepared a g-C₃N₄-based novel photocatalyst from melamine and urea. Briefly, 7.704 g urea, 5.4 g melamine, and different amount of ammonium chloride (NH₄Cl) were added to 90 mL deionized water. After stirring the solution for 30 min, it was dried at 80 °C to obtain the precursor powder. Then, the precursor powder was calcinated at 550 °C for 3 h at the heating rate of 0.5 °C/min. The whole schematic of the preparation of the Cl-doped g-C₃N₄ nanosheet catalyst is shown in Figure 1. Smykalova et al. [15] produced exfoliated g-C₃N₄ catalyst using melamine as the precursor.

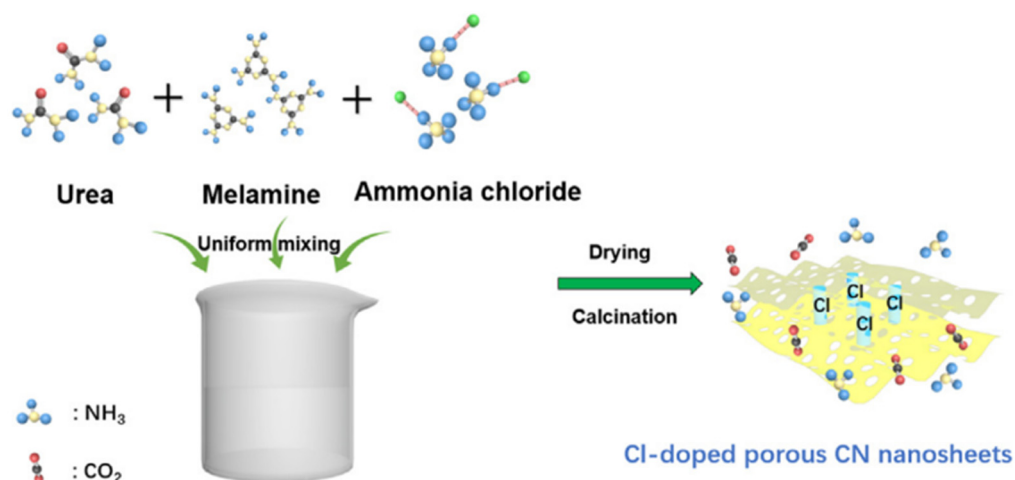


Figure 1. Schematic illustration of the preparation for Cl-doped porous CN nanosheets [14].

He et al. [16] prepared g-C₃N₄ powder from dicyanodiamine. Sixteen grams of dicyanodiamine was heated at the rate of 2.5 °C up to 600 °C and it was maintained for 4 h. After that, the heated powder was cooled and ground for further use. Wang et al. [17] also reported the preparation of g-C₃N₄ from dicyandiamide as the precursor. Sun et al. [18] produced bulk g-C₃N₄ from dicyandiamide as the precursor. To the prepared g-C₃N₄, kaolinite was loaded via the impregnation calcination process and the composite thus produced was named as g-C₃N₄/kaolinite (KCN). To it, Ag was loaded to form the ternary composite Ag/g-C₃N₄/kaolinite composite. The preparation procedure is illustrated in Figure 2.

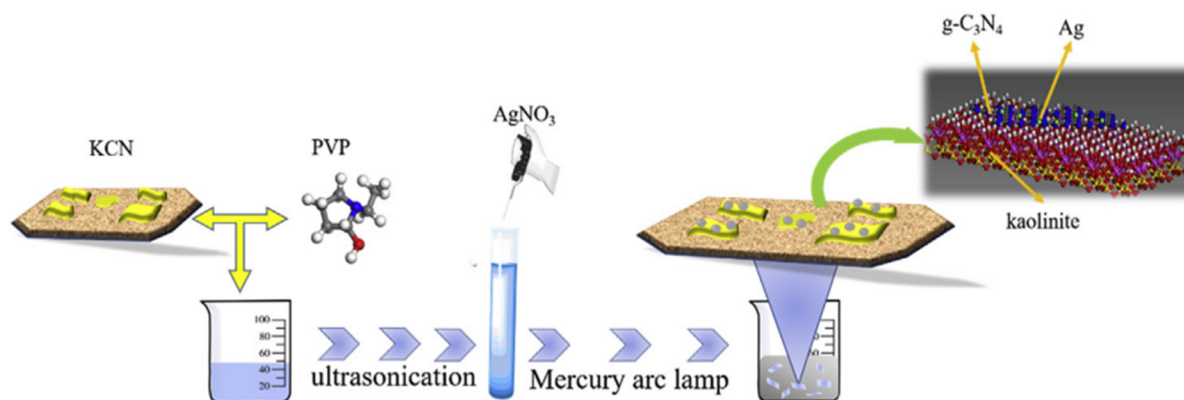


Figure 2. Scheme of the synthetic process for the Ag/KCN-X photocatalysts [18].

2.2. Composite with Other Materials

Often $g\text{-C}_3\text{N}_4$ is utilized in making composite catalysts with other suitable materials. ZnO is an excellent semiconductor photocatalyst material and has been proven to be an efficient catalyst for degrading different categories of PCs. Its bandgap is 3.2 eV and there is a huge possibility of electron–hole recombination. Along with this, its optical corrosion is another major hindrance behind its usage for real field purposes. In this regard, composite with $g\text{-C}_3\text{N}_4$ offers a sustainable efficient photocatalyst with higher activity. Feyzi et al. [19] prepared ZnO/ $g\text{-C}_3\text{N}_4$ /zeolite P supported photocatalyst for photodegradation of the tetracycline (TC) molecule. The composite catalyst was synthesized in three steps. Firstly, ZnO was prepared by the sol–gel method. Then $g\text{-C}_3\text{N}_4$ was synthesized at a large scale by means of pyrolysis of urea. In the final step, the as-synthesized ZnO and $g\text{-C}_3\text{N}_4$ were mixed and added to zeolite for the production of the composite catalyst. Mirzaei et al. [20] synthesized a ZnO@ $g\text{-C}_3\text{N}_4$ catalyst for the mineralization of a sulfamethoxazole (SMX) drug. Baladi et al. [21] reported the preparation and application of $g\text{-C}_3\text{N}_4\text{-CoFe}_2\text{O}_4\text{-ZnO}$ photocatalyst for the degradation of the penicillin G antibiotic compound. Chen et al. [22] applied Ag-AgVO₃/ $g\text{-C}_3\text{N}_4$ photocatalyst for the degradation of TC antibiotic. $g\text{-C}_3\text{N}_4/\text{TiO}_2/\text{CFs}$ composite was synthesized by Guo et al. for TC elimination from wastewater [23]. Firstly, different quantity of oxamide and 10 g of urea were blended mechanically. After that, the mixture was subjected to calcination in a muffle furnace at 550 °C to produce $g\text{-C}_3\text{N}_4$. In order to synthesize the $g\text{-C}_3\text{N}_4/\text{TiO}_2$ composite, the as-prepared $g\text{-C}_3\text{N}_4$ was dissolved in a previously prepared Ti(SO₄)₂ solution and the whole setup was subjected to ultra-sonification. The whole process was repeated in the presence of carbon fibers (CFs) to prepare the composite $g\text{-C}_3\text{N}_4/\text{TiO}_2/\text{CFs}$. Kumar et al. [24] deployed BiOCl/ $g\text{-C}_3\text{N}_4/\text{Cu}_2\text{O}/\text{Fe}_3\text{O}_4$ ternary composite photocatalyst for oxidative degradation of SMX from wastewater.

2.3. Doping of $g\text{-C}_3\text{N}_4$ -Based Catalysts

Doping and co-doping with various metals and metal oxides enhanced the catalytic activity of $g\text{-C}_3\text{N}_4$ -based materials. Wang et al. [25] investigated the co-doping of bimetallic oxides and the effect of oxygen on the catalytic degradation performance of $g\text{-C}_3\text{N}_4$ on SMX removal. Liang et al. [26] prepared Ba-atom-embedded $g\text{-C}_3\text{N}_4$ -based catalyst for the degradation of carbamazepine (CBZ) and DC drug molecules. The Ba atom got anchored onto the surface of the $g\text{-C}_3\text{N}_4$ by means of forming an ionic bond with the triazine ring. The catalyst was prepared by the thermal polymerization method. In this method, 2.52 g melamine was mixed with 60 mL of ethylene glycol. This solution was kept in the temperature range of 58–62 °C and was named as solution A. On the other hand, 28% 5 mL HNO₃ was prepared and named as solution B, and 40 mL of Ba(NO₃)₂ (in the range of 10–25 mmol) solution as solution C. These three solutions (A, B, and C) were mixed to form a white hydrogel and allowed to stand for 1 h. Then it was filtered and washed thoroughly with ethanol. The solid residue was heated at 550 °C to produce the Ba-embedded $g\text{-C}_3\text{N}_4$ catalyst. Tian et al. [27] prepared a Se-doped $g\text{-C}_3\text{N}_4$ novel catalyst for SMX detoxification. Due to Se doping, nitrogen vacancy is created in the catalyst matrix to modulate the electron distribution of $g\text{-C}_3\text{N}_4$. Additionally, it also helped in exfoliation and creating a large specific surface area of the composite catalyst due to the large radius of the Se atom. Guo et al. [14] reported the preparation and application of a Cl-doped novel porous $g\text{-C}_3\text{N}_4$ nanosheet photocatalyst for TC degradation under the irradiation of visible light. For doping purposes, different amounts of Cl were added, and the composite was named accordingly as CN-Cl-0.1, CN-Cl-0.3, CN-Cl-0.5, etc.

3. Different Categories of $g\text{-C}_3\text{N}_4$ -Based Catalysts Reported in the Literature for PC Degradation

It has been already mentioned in the previous section that although $g\text{-C}_3\text{N}_4$ is a promising photocatalytic material, several drawbacks hinder its application. Therefore, researchers look forward to constructing different types of composite materials for en-

hanced photocatalytic activity. The main purpose of developing a novel g-C₃N₄-based photocatalyst is to reduce the bandgap and prevent the electron–hole recombination. For this purpose, photocatalysts having Z-scheme and S-scheme heterostructures are synthesized. Most of the g-C₃N₄-based catalysts have been found to be efficient under visible light irradiation. However, in some cases, the inclusion of some external agents, such as H₂O₂, peroxymonosulfate (PMS), and ultrasound assistance, facilitates the degradation process.

3.1. g-C₃N₄-Based Z-Scheme Photocatalysts

Z-scheme photocatalysts can be categorized into traditional Z-scheme, direct Z-scheme, and all-solid-state Z-scheme photocatalysts. Traditional Z-scheme photocatalysts were first introduced by Bard in 1979 [28]. It resembles the photosynthetic activity performed by green plants. This type of photocatalysts consists of two semiconductors with suitable intermediate couples. The two semiconductors used in this system have staggered band structure configurations. However, the major disadvantage of this type of catalyst is that it is confined to the solution phase only. Moreover, there is also a possibility of the occurrence of many side reactions.

All-solid-state Z scheme is also known as the indirect Z scheme. The idea of the all-solid-state Z scheme started in the year of 2006. Tada et al. [29] synthesized CdS-Au-TiO₂ ternary composite photocatalyst. In this composite, Au acts as the electron mediator. Noble metals, such as Ag, Au, and Cu nanoparticles, are often explored as the electron mediator. Other than these, carbon quantum dots, graphene, and carbon nanotubes are also used as the electron mediator. As the solid conductor is used in all-solid-state Z scheme, it can be easily utilized in liquid as well as in gas.

However, in all-solid-state Z-scheme-based catalysts, charge transfer is solely based on the conductor. To improve the situation, a direct Z scheme was proposed. In the direct Z-scheme mechanism, no intermediate redox couples exist. Many recent studies on the application of g-C₃N₄-based catalysts are developed based on a direct Z-scheme mechanism. The photodegradation of TC by applying 2D/2D MnIn₂S₂/g-C₃N₄ composite is based on the direct Z-scheme mechanism [30]. Photodegradation of DC via S, B-co-doped g-C₃N₄ nanotube@MnO₂ catalyst also proceeded via a direct Z-scheme mechanism [3]. The main reactive species involved in the degradation mechanism were h⁺, O₂^{·-}, and SO₄^{·-}. Moreover, the catalyst showed excellent stability up to 10 cycles. Ghosh and Pal [8], in their recent work, reported the synthesis and application of composite formed by g-C₃N₄ nanosheet, tungsten oxide hydrate nanoplates, and carbon quantum dots towards TC degradation under visible light exposure. It worked on the principle of all-solid-state Z schemes, and the degradation proceeded with a rate constant of 0.044 min⁻¹.

3.2. g-C₃N₄-Based S Scheme Photocatalysts

S scheme is the other name of the step scheme photocatalyst. An S scheme photocatalyst comprises an oxidation photocatalyst and a reduction photocatalyst with a staggered band structure. Its band structure is similar to that of the type II heterojunction but a completely different charge transfer route. Pham et al. [31] prepared S scheme α-Fe₂O₃/g-C₃N₄ nanocomposites as an efficient photocatalyst for the degradation of model antibiotic compounds, such as amoxicillin (AMX) and cefalexin (CFX). Ni et al. [32] prepared a novel g-C₃N₄/TiO₂ catalyst for TCH degradation under UV light irradiation. The S-scheme heterostructure facilitated the formation of ·O₂⁻, h⁺, and OH· reactive species which ultimately helped in degradation performance. Feyzi et al. [19] reported the application of S-scheme ZnO/g-C₃N₄/zeolite P supported catalyst for the degradation of TC molecule. The ternary composite catalyst was loaded on a plasma reactor for degradation purposes. Under optimized reaction conditions, 95.5% degradation efficiency was achieved. Guo et al. [23] synthesized an S-scheme-based novel g-C₃N₄/TiO₂/CFs catalyst for the photocatalytic degradation of TCH. Under 350 W Xe light irradiation, 99.9% degradation was achieved within 90 min.

3.3. *g-C₃N₄-Based Fenton-Type Catalysts*

Fenton-type reactions are one of the powerful techniques for the degradation of organic pollutants. It deploys the generation of powerful hydroxyl radicals from H₂O₂ in the presence of Fe²⁺ as the catalyst. However, there exists a lot of technical problems with the homogeneous Fenton process and therefore, the scientists are continuously developing novel heterogeneous Fenton catalysts for degradation purposes. There are several reported studies on the application of heterogeneous Fenton catalysts for PC wastewater degradation. It is very important to note that *g-C₃N₄* undoubtedly added a new dimension for synthesizing heterogeneous Fenton-type catalysts. In the traditional Fenton process, iron was used as the catalyst, and H₂O₂ was the oxidant. However, apart from iron, different other transition metals have also been explored as Fenton-type catalysts. Moreover, PMS has replaced H₂O₂ in many studies. Moreover, visible light irradiation also often enhances degradation and is known as photo-Fenton degradation. This section describes different Fenton, Fenton types, and PMS-mediated *g-C₃N₄*-based catalysts for PC degradation.

Zhang et al. [33] reported the application of MnO₂/Mn-modified alkalized *g-C₃N₄* catalyst for TC degradation through the photo-Fenton process. Excellent degradation (96.7%) occurred due to the synergistic effect of the surface-grafted hydroxyl groups, charge transfer via the Z-scheme mechanism, and activation of H₂O₂ by the redox cycle of Mn(IV)/Mn(III)/Mn(II). He et al. [16] utilized *g-C₃N₄/Fe₃O₄@MIL-100(Fe)* composite for photo-Fenton detoxification of CIP from wastewater. In comparison to the bare *g-C₃N₄* and *Fe₃O₄@MIL-100(Fe)*, the composite catalyst showed promising performance, exhibiting 94.7% degradation of CIP and having an initial concentration of 200 mg/L in 120 min.

Mei et al. [34] explored a metal-free carboxyl-modified *g-C₃N₄* catalyst for PMS activation in order to degrade model PC, CBZ. As the process did not involve any strong acids or solvents, it has been described as a green low-cost environmentally friendly system. Luo et al. [35] reported the successful application of a Co-MOF-based/*g-C₃N₄* catalyst for degrading antidepressant PC venlafaxine in the presence of PMS. Wang and Wang [36] studied the degradation process of SMX in the presence of γ -Fe₂O₃/*O-g-C₃N₄*/biochar composite via PMS activation. SMX eradication followed a first-order kinetic model with a rate constant value of 0.153 min⁻¹. Wang et al. [25] utilized a Fe-Co-O-co-doped *g-C₃N₄* catalyst for PMS activation in order to degrade SMX molecules. Detailed experimental investigation revealed that both sulfate radical and singlet oxygen were present in the reaction mixture. However, the role of singlet oxygen in the SMX removal process was not clear. Superb degradation efficiency was attributed to the existence of the synergism between the metal oxide and *O-g-C₃N₄*.

Liu et al. [37] developed a novel Z-scheme Fe-*g-C₃N₄*/Bi₂WO₆ heterogeneous photo-Fenton catalyst for TC degradation purposes. Experimental investigation revealed that ¹O₂ and [•]O₂⁻ were the predominant species participating in the degradation phenomenon. Li et al. [38] prepared a *g-C₃N₄/MgO* composite which acted as a Fenton-type catalyst for the oxidation of the SMX drug present in wastewater. The composite catalyst showed excellent performance towards the degradation. The H₂O₂ requirement was also less for oxidative degradation.

Li and Gan [39] applied Cu-doped *g-C₃N₄* composite as the heterogeneous photo-Fenton-type catalyst for the degradation of different PCs at a very low concentration. Due to the doping, the bandgap got reduced from 2.79 eV to 2.17 eV, which proved beneficial for adsorbing visible sunlight for degradation purposes. Cao et al. [40] synthesized novel Fe/*g-C₃N₄*/kaolinite as the heterogeneous photo-Fenton catalyst for TCH degradation purposes. High degradation efficiency was achieved due to the large specific surface area of the kaolinite, which can result in the adsorption of the TCH molecule. Moreover, Fe(III) acted as the electron acceptor in the composite matrix, restricted the electron-hole recombination rate, and facilitated the photo-Fenton process. *g-C₃N₄* nanosheets/schwertmannite nanocomposites were explored by Qiao et al. [41] for chlortetracycline eradication from wastewater through the photo-Fenton mechanism.

3.4. *g*-C₃N₄-Based Sonocatalysts for PCs Degradation

Ultrasound is often deployed for the destruction of stable organic molecules in wastewater streams. Experimentally it has been proved that sound waves having a frequency greater than 20 kHz have the capability of breaking organic pollutants of higher molecular weight into simpler products. Some *g*-C₃N₄-based sonocatalysts have also been reported in the literature related to the degradation of PCs. Zhang et al. [42] utilized CoFe₂O₄/*g*-C₃N₄ composite as the sonocatalyst for the degradation of the TCH molecule. Maximum sonocatalytic efficiency of 26.71% in 10 min was exhibited by the composite catalyst when the amount of CoFe₂O₄ in the catalyst matrix was 25%. Charge transfer and electron–hole separation mechanism proceeded via S scheme heterojunction. The mechanism is shown in Figure 3.

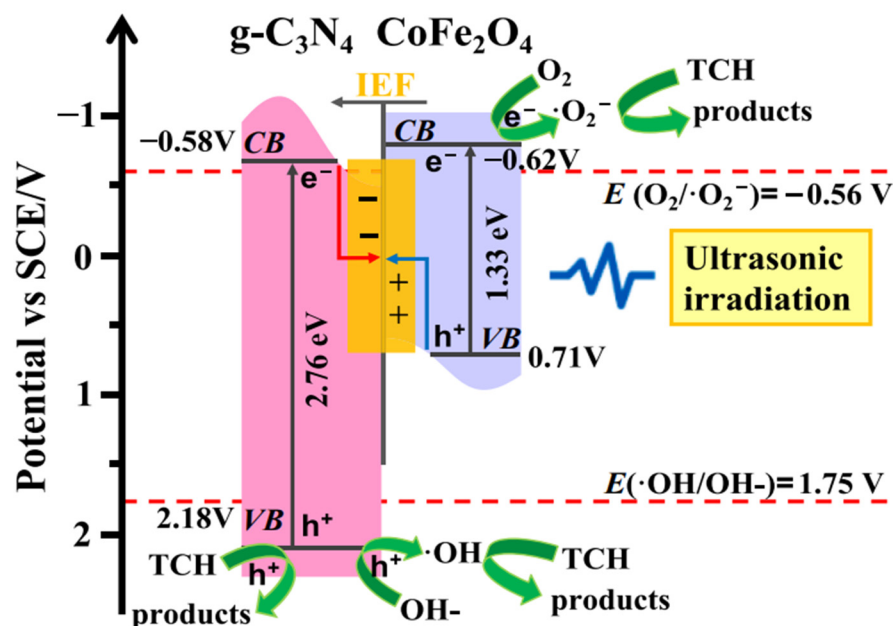


Figure 3. Proposed mechanism for the sonocatalytic degradation of TCH with CFO/CN [42].

He et al. [43] prepared *g*-C₃N₄/MoS₂ catalyst for levofloxacin (LFX) oxidation through a sonocatalytic mechanism. The as-prepared catalyst showed excellent degradation efficiency towards LFX (75.81%) with an initial concentration of 10 mg/L in 140 min with promising reusability. Experimental investigation revealed that both ·OH and ·O₂⁻ played a major role in the degradation process. The authors validated the sonocatalytic degradation via hotspot and sonoluminescence effect theory.

Vinesh et al. [44] described the application of r-GO supported *g*-C₃N₄ nanosheet catalyst for sonophotocatalytic degradation of TC. Influence of ultrasound generated more active sites in the catalyst, which ultimately improved PC degradation. For a TC sample having a 15 mg/L initial concentration, almost 90% degradation was achieved within 60 min of reaction under sonophotocatalysis. Gholami et al. [45] applied Zn-Cu-Mg mixed metal hydroxide/*g*-C₃N₄ composite as the effective sonophotocatalyst for the degradation of sulfadiazine (SDZ) drug from wastewater. When the content of mixed metal hydroxide remained at 15 wt%, maximum degradation efficiency of 93% was attained with an initial concentration of SDZ as 0.15 mM, solution pH 6.5, and ultrasonication power of 300 W.

4. Degradation of Different PCs

4.1. Tetracycline (TC)

TC is one of the most common drugs, often explored to test the catalytic efficiency of a newly developed catalyst. It is a broad-spectrum antibiotic. Its major functional groups include phenolic hydroxyl group, dimethylamino group, acylamino group, etc. Owing to

the possession of both electron-rich and electron-deficit groups, it has three dissociation constants [1]. TC, OTC (oxytetracycline), and TCH (tetracycline hydrochloride) all belong to the TC group of drugs. Chen et al. [22] explored Ag-AgVO₃/g-C₃N₄ photocatalyst for the degradation of TC in aqueous media. The photocatalytic activity of the composite catalyst was two times higher than that of the pristine g-C₃N₄. A highly promising MnIn₂S₄/g-C₃N₄ photocatalyst was developed by Chen et al. [30] and successively applied for TCH degradation. The composite catalyst exhibited higher degradation efficiency in comparison to the MnIn₂S₄ nanoflakes and mesoporous g-C₃N₄ nanosheets. The enhanced removal occurred due to the formation of the Z scheme which results in the transfer and effective separation of the photogenerated charge carriers. Chi et al. [13] reported the exploration of B/Na-co-doped g-C₃N₄ photocatalyst for the degradation of TC. The synergistic effect between the B/Na co-doping and the porous g-C₃N₄ nanosheet played a major role in the degradation process. Within a reaction time of 30 min, under visible light irradiation ($\lambda = 430$ nm), 78.39% degradation was achieved. Cl-doped g-C₃N₄-based catalysts were explored by Guo et al. [14] for TC degradation purposes. The optimized removal efficiency of 92% within 120 min of reaction time has been achieved. Due to the Cl doping, the electronic structure of g-C₃N₄ material was regulated. Moreover, because of the Cl doping, the specific surface area of the composite got increased and the recombination of hole-electrons on the catalyst surface was prevented. Thus ultimately, TC degradation was improved in comparison to the bulk g-C₃N₄ catalyst.

Jiang et al. [46] developed a nitrogen self-doped g-C₃N₄ nanosheet catalyst following a self-doping and thermal exfoliation procedure. Thus, the newly developed nitrogen-doped g-C₃N₄ photocatalyst showed enhanced visible light absorption, high specific surface area, and improved electron-hole separation in comparison to the bulk g-C₃N₄. Hence, it showed promising efficiency towards TC degradation. The authors proposed an interesting mechanism behind the photocatalytic degradation of TC. The whole degradation process progressed via three steps, such as light harvesting, photogenerated electron-hole pairs separation and transfer, and surface adsorption and redox reaction. Moreover, the catalyst showed excellent repeatability and only a negligible efficiency is lost during the fifth cycle of reuse.

Palanivel et al. [47] reported the synthesis of a novel NiFe₂O₄-deposited S-doped g-C₃N₄ nanorod catalyst and deployed it for TC degradation through a photo-Fenton mechanism. Strong chemical interaction between the NiFe₂O₄ and sulfur-doped g-C₃N₄ helps in efficient visible light absorption, and electron-hole recombination is also prevented effectively. Preeyangha et al. [48] prepared g-C₃N₄/BiOBr/Fe₃O₄ nanocomposite photocatalyst for the degradation of TC under the irradiation of visible light. Complete degradation and 78% TOC removal were achieved within 60 min, where the reaction rate constant was found six times higher than that obtained with the bare g-C₃N₄ catalyst. Based on the radical scavenging investigations, it was observed that h⁺ has a major role in the degradation followed by ·O₂⁻ and OH·. Besides that, the ternary composite showed excellent recyclability also. The possible reaction mechanism is shown in Figure 4.

Various reported g-C₃N₄-based catalysts for TC removal are presented in Table 1.

Table 1. A list of g-C₃N₄-based catalysts reported for TC degradation.

Description of the g-C ₃ N ₄ -Based Photocatalyst	Optimized Degradation Efficiency with Reaction Condition	References
B/Na-co-doped porous g-C ₃ N ₄ nanosheet photocatalyst	TC degradation of 78.39% within 30 min under visible light irradiation (10 W LED lamp)	[13]
Cl-doped porous g-C ₃ N ₄ nanosheets	At a catalyst dose of 0.5 g/L, TC concentration = 10 mg/L, under visible light irradiation (300 W Xenon lamp, with cut-off filter at 420 nm), 92% degradation within 120 min reaction time	[14]
ZnO/g-C ₃ N ₄ /zeolite P supported catalyst	95.5% TC degradation in plasma reactor (16.5 kV as operating voltage, 300 Hz regulated frequency, airflow rate = 130 mL/min)	[19]

Table 1. Cont.

Description of the g-C ₃ N ₄ -Based Photocatalyst	Optimized Degradation Efficiency with Reaction Condition	References
Ag-AgVO ₃ /g-C ₃ N ₄ composite	83.6% degradation at 120 min (rate constant = 0.0298 min ⁻¹) under visible light irradiation (300 W Xenon lamp, with 410 nm filter): TC concentration = 30 mg/L, catalyst dose = 0.2 g/L	[22]
g-C ₃ N ₄ /TiO ₂ /CFs	99.99% TC-HCl degradation (initial concentration = 10 mg/L) with a catalyst dose of 0.5 g/L, under the irradiation of visible light (350 W Xe lamp) for 90 min	[23]
MnIn ₂ S ₄ /g-C ₃ N ₄ photocatalyst	With TCH concentration of 50 mg/L, catalyst dose = 1 g/L (g-C ₃ N ₄ kept as 20% mass ratio in the composite), under visible light irradiation (300 W Xenon lamp, with 400 nm filter) almost complete degradation	[30]
g-C ₃ N ₄ /TiO ₂	In the presence of catalyst (g-C ₃ N ₄ :TiO ₂ = 1:25) at a dose = 1 g/L, under UV light irradiation (300 W Mercury lamp), maximum degradation efficiency obtained 97.6% for TCH in 90 min	[32]
Porous Z-scheme MnO ₂ /Mn-modified alkalized g-C ₃ N ₄ heterojunction	With 0.5 g/L catalyst dose, 96.7% TC removal	[33]
Fe-g-C ₃ N ₄ /Bi ₂ WO ₆ heterojunctions	98.42% degradation in the presence of 1 mM of H ₂ O ₂ , with TC = 10 mg/L, catalyst dose = 0.4 g/L, solution pH = 6.5	[37]
rGO supported self-assembly of 2D nanosheet of (g-C ₃ N ₄)	With 0.25 g/L catalyst dose, TC concentration = 15 mg/L, almost complete degradation (under visible light irradiation and exposure to ultrasound)	[44]
Nitrogen self-doped g-C ₃ N ₄ nanosheets	With 0.5 g/L catalyst dose, 10 mg/L TC concentration, under visible light irradiation, 81.67% degradation in 60 min	[46]
NiFe ₂ O ₄ -deposited S-doped g-C ₃ N ₄ nanorod	97% degradation in 60 min under visible light irradiation	[47]
g-C ₃ N ₄ /BiOBr/Fe ₃ O ₄ nanocomposite	With catalyst dose = 0.5 g/L, TC = 15 mg/L, under visible light irradiation (300 W Halogen lamp), complete degradation in 60 min	[48]
Ba-doped g-C ₃ N ₄ photocatalyst	91.94% TC degradation within 120 min under visible light irradiation at 2% Ba loading at a solution pH 10	[49]
g-C ₃ N ₄ /MoS ₂ p-n heterojunction photocatalyst	Using photocatalyst dose of 1 g/L, TC concentration of 20 mg/L, irradiation under Xe lamp (300 W) complete degradation achieved within 40 min (rate constant = 547 × 10 ⁻⁴ min ⁻¹)	[50]
PdO/g-C ₃ N ₄ /kaolinite catalyst	At 4% loading of PdO, catalyst dose (0.5 g/L) 94.5% degradation of TCH (40 mg/L) by PMS activation under visible light (300 W Xenon lamp, with 420 nm cut-off filter) irradiation within 20 min	[51]
Nitrogen-doped carbon quantum dots modified g-C ₃ N ₄ composite	90% TCH degradation under the action of 0.5 g/L catalyst dose, TCH concentration = 20 mg/L, peroxydisulphate (PDS) dose = 0.5 g/L, under visible light irradiation (300 W Xenon lamp, with 420 nm cut-off filter) within 60 min reaction time	[52]
CoO/g-C ₃ N ₄ p-n heterojunction	Initial concentration of TC = 10 mg/L, catalyst dose = 0.5 g/L (30 wt% CoO), 90% degradation within 60 min under visible light irradiation (300 W Xenon lamp, with cut-off filter at 420 nm)	[53]
CuInS ₂ /g-C ₃ N ₄ heterojunction photocatalyst	83.7% degradation within 60 min, initial concentration of TC = 20 mg/L, catalyst dose = 0.5 g/L (CuInS ₂ mass = 50 wt%) under visible light irradiation (300 W Xenon lamp, with cut-off filter at 420 nm)	[54]

Table 1. Cont.

Description of the g-C ₃ N ₄ -Based Photocatalyst	Optimized Degradation Efficiency with Reaction Condition	References
CoP nanoparticles anchored on g-C ₃ N ₄ nanosheets	96.7% degradation within 120 min reaction time under visible light irradiation (500 W Xenon lamp with 520 nm cut-off filter)	[55]
g-C ₃ N ₄ /RGO/In ₂ S ₃	With initial TCH concentration = 20 mg/L, catalyst dose = 0.5 g/L, 95.6% degradation in 60 min under visible light irradiation	[56]
Metal-free g-C ₃ N ₄ -based heterojunction photocatalyst	Catalyst dose of 2 g/L, TC concentration = 20 mg/L, under visible light irradiation (300 W Xe lamp with 420 nm filter) 91% removal in 100 min	[57]
Bi _x O _y I _z /g-C ₃ N ₄	TCH concentration = 10 mg/L, under visible light irradiation (500 W Xe lamp with 420 nm filter), 40% degradation in 4 h	[58]
Bi ₂ W ₂ O ₉ /g-C ₃ N ₄ heterojunction	2wt% Bi ₂ W ₂ O ₉ in the matrix, with 1 g/L catalyst dose, with initial concentration of TCH = 10 mg/L, under visible light irradiation (35 W Xe lamp), at pH 10.54, 95% degradation occurred	[59]
Carbon-doped g-C ₃ N ₄	More than 95% degradation in 90 min reaction time under visible light irradiation	[60]
Single-atom Fe-g-C ₃ N ₄ catalyst	With TC concentration = 10 mg/L, catalyst dose = 0.1 g/L, PMS = 0.25 mM, 93.29% degradation achieved	[61]
Ag-modified g-C ₃ N ₄ composite	With 8 wt% Ag in the matrix, 1 g/L catalyst dose, 20 mg/L TC concentration, under visible light irradiation (300 W Xe lamp, with 420 nm filter), at pH 11, 90% degradation achieved	[62]
g-C ₃ N ₄ /Ag ₂ CrO ₄ photocatalyst	With catalyst dose 1 g/L, TC concentration = 10 mg/L, under visible light irradiation (1000 W halogen lamp), almost complete degradation in 180 min	[63]
FeOOH coupling and nitrogen vacancies functionalized g-C ₃ N ₄ heterojunction	With 4 g/L catalyst dose, initial concentration of OTC = 10 mg/L, under visible light irradiation (300 W Xe lamp, with 420 nm filter), 92.83% degradation in 90 min	[64]
Co-doped KCl/NH ₄ Cl/g-C ₃ N ₄ catalyst	With catalyst dose = 1 g/L, TC concentration = 10 mg/L, under visible light irradiation (500 W Xe lamp with 420 nm filter), almost complete degradation in 120 min	[65]
Potassium-gluconate-cooperative pore generation based on g-C ₃ N ₄ nanosheets	With catalyst dose = 1 g/L, TC concentration = 20 mg/L, under visible light irradiation (300 W Xe lamp, with 420 nm filter), 82.2% degradation in 30 min	[66]
Sulfur-doped carbon quantum dots loaded hollow tubular g-C ₃ N ₄	With catalyst dose = 1 g/L, TC concentration = 20 mg/L, under visible light irradiation (300 W Xe lamp), about 90% degradation in 60 min	[67]
Nano-confined g-C ₃ N ₄ in mesoporous SiO ₂	With 0.33 g/L catalyst dose, TC concentration = 20 mg/L, under visible light irradiation (300 W Xe lamp), complete degradation in 120 min	[68]
Multifunctional 2D porous g-C ₃ N ₄ nanosheets hybridized with 3D hierarchical TiO ₂ microflowers	With 0.5 g/L catalyst dose, TC concentration = 20 mg/L, under visible light irradiation, 90% degradation achieved in 60 min	[69]
CuO/g-C ₃ N ₄ 2D/2D heterojunction photocatalysts	With catalyst dose of 0.1 g/L, 30 mg/L OTC, under visible light irradiation (300 W Xe lamp, with 420 nm filter), 100% degradation in 10 min	[70]
Sulfur- and tungstate-co-doped porous g-C ₃ N ₄ microrods	With 0.5 g/L catalyst dose, TC concentration of 10 mg/L, under visible light irradiation (300 W Xe lamp, with 420 nm filter), 85.3% degradation in 120 min	[71]
Supramolecular self-assembly synthesis of noble-metal-free (C, Ce) co-doped g-C ₃ N ₄ with porous structure	With 0.5 g/L catalyst dose, 10 mg/L TC concentration, 90% degradation in 60 min	[72]

Table 1. Cont.

Description of the g-C ₃ N ₄ -Based Photocatalyst	Optimized Degradation Efficiency with Reaction Condition	References
Bi ₂ O ₂ CO ₃ /g-C ₃ N ₄ / Bi ₂ O ₃	With catalyst dose = 0.2 g/L, TC = 10 mg/L, under visible light irradiation (300 W Xe lamp), 95% degradation in 60 min	[73]
Fe-doped surface-alkalinized g-C ₃ N ₄	With catalyst dose = 0.5 g/L, TC concentration = 20 mg/L, under visible light irradiation (300 W Xe lamp), 70% degradation in 80 min	[74]
Donor–acceptor structured g-C ₃ N ₄	With 0.5 g/L catalyst dose, OTC concentration = 20 mg/L, degradation of 93% at 60 min	[75]
C-doped g-C ₃ N ₄ /WO ₃	With catalyst dose = 1 g/L, TC concentration = 10 mg/L, under visible light irradiation (500 W Xe lamp with 420 nm filter), ~78% degradation in 60 min	[76]
g-C ₃ N ₄ /NiFe ₂ O ₄ S scheme	79.3% degradation at pH 3	[77]

4.2. Diclofenac (DC)

DC is also another drug like TC which is also investigated by researchers for degradation purposes. It is one of the notable members of the nonsteroidal anti-inflammatory drug group possessing high K_{ow} and bioaccumulating potential power. Due to its wide unrestricted usage during the last four decades, it has become one of the significant emerging contaminants of the current era. Various reports are available in the literature describing the applicability of g-C₃N₄-based photocatalysts towards sustainable eradication of DC from wastewater. Li et al. [78] applied Fe oxide nanoclusters supported on g-C₃N₄ as a robust photocatalyst for DC degradation purposes. He et al. [4] prepared a heterostructure of Ti₃C₂/g-C₃N₄ photocatalyst for the degradation of DC. Polymeric g-C₃N₄ catalyst was explored by Papamichail et al. [79] for degradation of DC. Quantum carbon dots modified reduced ultrathin g-C₃N₄ photocatalyst was designed and applied by Jin et al. [80] for the oxidative degradation of DC from wastewater. Complete degradation of DC took place within 6 min. Hu et al. [81] deployed g-C₃N₄/TiO₂ photocatalyst for the degradation of DC and CBM. The mechanism is shown in Figure 5.

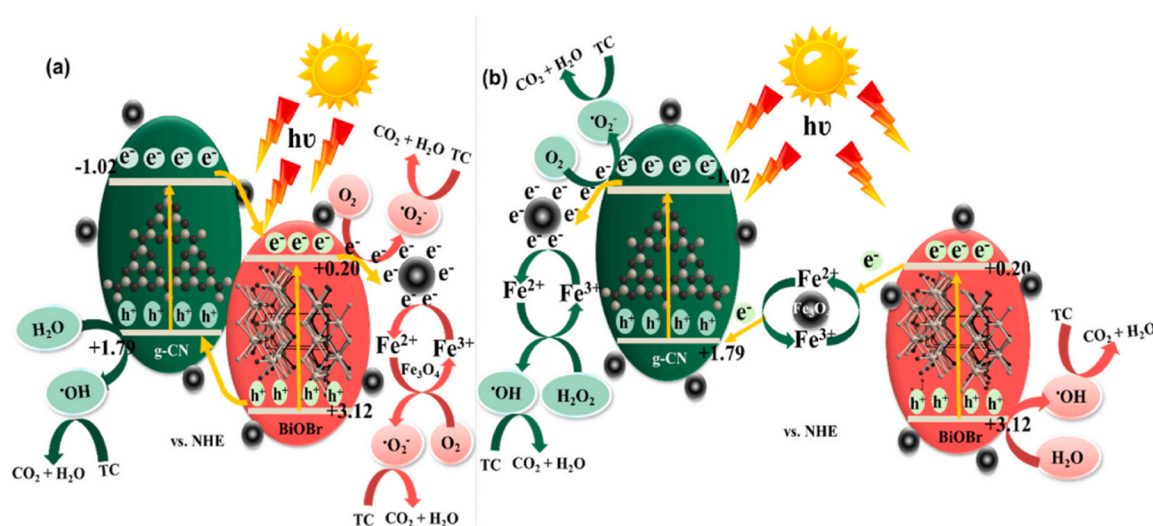


Figure 4. The schematic representation of plausible charge transfer mechanism (a) type II and (b) Z-scheme heterojunction during the photocatalytic TC degradation over g-CN/BiOBr/Fe₃O₄ nanocomposites [48].

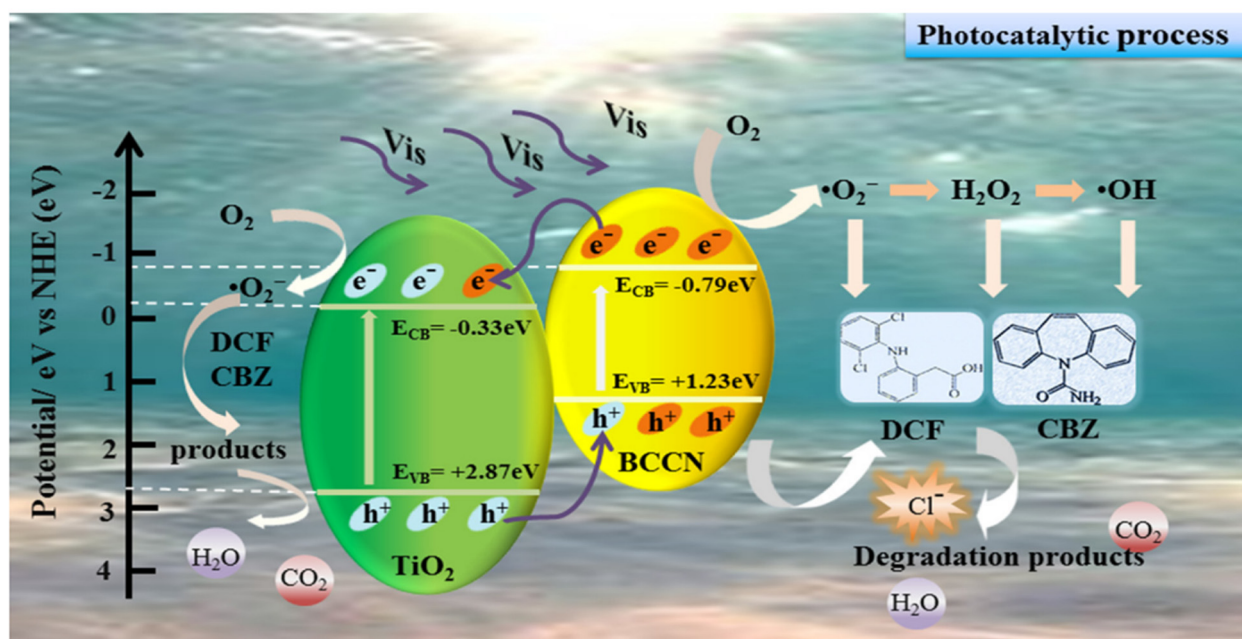


Figure 5. Possible mechanism for the photodegradation of DCF and CBZ under LED lamp irradiation over 30% BCCNT composites [81].

A comprehensive list regarding the application of different g-C₃N₄-based photocatalysts for the degradation of DC is provided in Table 2.

Table 2. A list of g-C₃N₄-based catalysts reported for DC degradation.

Description of the Catalyst	Reaction Conditions for Optimum Degradation Efficiency	Optimized Degradation Efficiency	References
Z-scheme S, B-co-doped g-C ₃ N ₄ nanotube@MnO ₂ heterojunction	In the presence of 0.06 mM PMS, photocatalyst dose of 0.5 g/L, DC concentration = 20 mg/L, under the irradiation of 8 × 8 W visible light lamps at a wavelength of 460 nm	99% degradation	[3]
2D/2D heterostructure of Ti ₃ C ₂ /g-C ₃ N ₄	Initial concentration of DC = 10 mg/L, catalyst dose = 0.25 g/L, PMS concentration = 0.25 g/L	100% degradation efficiency within 30 min	[4]
Ferric oxide nanoclusters anchored g-C ₃ N ₄ nanorods	Initial concentration of DC = 1 mg/L, dose of catalyst = 0.1 g/L, irradiation under 300 W Xenon arc lamp	Kinetic rate constant of 0.206 min ⁻¹	[78]
Polymeric g-C ₃ N ₄ photocatalyst	At a catalyst dose of 1 g/L, initial concentration of DC = 20 mg/L, solution pH = 5	Complete removal within 120 min	[79]
TiO ₂ /g-C ₃ N ₄	Initial concentration of DC = 5 mg/L, 0.3 g of catalyst loading, pH = 5, irradiation under 1000 W halogen lamp	Maximum degradation efficiency of 93.49%	[82]
Cellulose biochar/g-C ₃ N ₄ composite (WPBC ₅₀ /g-C ₃ N ₄)	At a DC concentration of 0.05 mM, catalyst dose of 1.5 g/L, 3 mM of PMS under visible light irradiation	Complete removal within 25 min	[83]
g-C ₃ N ₄ nanosheets	Initial concentration of DC = 3 mg/L, catalyst dose = 0.65 g/L under solar and LED irradiation	-	[84]
Tunable V ₂ O ₅ /boron-doped g-C ₃ N ₄ composite	With 5 wt% B doping, 2 g/L catalyst dose	100% degradation within 105 min under visible light irradiation	[85]
g-C ₃ N ₄ /NH ₂ -MIL-125 photocatalyst	Under the action of the catalyst composed of MOF and g-C ₃ N ₄ in the ratio 50:50. DC concentration kept at 10 mg/L, under UV LED irradiation at 384 nm	Complete eradication within 2 h	[86]

4.3. Sulfamethoxazole (SMX)

SMX is another widely used sulfonamide antibiotic. Due to its overuse, it often comes across in different quantities in different water bodies. In recent years, several studies report the catalytic elimination of sulfamethoxazole from water bodies by deploying g-C₃N₄-based composite catalysts. ZnIn₂S₄/g-C₃N₄ photocatalyst was utilized by Reddy et al. [87] to catalytically degrade SMX in a water medium. Tian et al. [27] fabricated a Se-doped g-C₃N₄ catalyst for the degradation of SMX through PMS activation. Experimental findings showed that 93% SMX can be degraded by the synthesized catalyst within 180 min with a reaction rate constant of 0.0149 min⁻¹. The rate constant of the doped catalyst was four times higher in comparison to the bulk g-C₃N₄ catalyst. The inclusion of Se in the composite matrix created nitrogen vacancy to modulate the electron distribution of the g-C₃N₄ catalyst. Peng et al. [88] utilized a “trap-zap” catalyst for the degradative elimination of SMX through PMS activation. β-Cyclodextrin polymer composite with Fe-doped g-C₃N₄ catalyst was used for the degradation. The degradation rate constant by the β-CDPs/Fe-g-C₃N₄ catalyst was found as 0.132 min⁻¹ which was 14.7 times and 2.2 times higher than that of the g-C₃N₄ and Fe-g-C₃N₄ catalyst. The inclusion of β-CDPs in the catalyst composition accelerated the electron transfer between the catalyst and PMS. Li et al. [89] applied a FeCo₂S₄-modified g-C₃N₄ catalyst for the degradation of the SMX drug. Optimized degradation efficiency has been obtained at the unadjusted pH of 6.5. On the other hand, acidic pH inhibited the degradation. Temperature played a major role in the degradation process. When the reaction temperature was increased from 10 °C to 40 °C, the degradation efficiency got enhanced from 61.2% to 99.9% with a rate constant value of 0.294 min⁻¹. The schematic for the mechanism is shown in Figure 6.

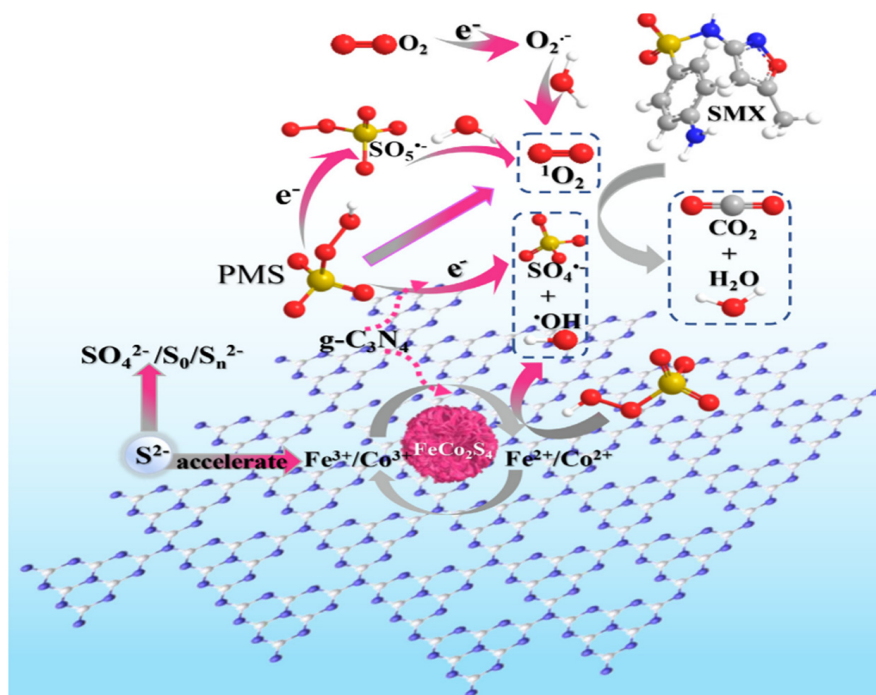


Figure 6. Schematic illustration of the mechanism of PMS activation on FeCo₂S₄-CN [89].

A comprehensive list regarding the application of different g-C₃N₄-based photocatalysts for the degradation of SMX is provided in Table 3.

Table 3. A list of g-C₃N₄-based catalysts reported for SMX degradation.

Description of the Catalyst	Reaction Condition	Optimized Degradation Efficiency	References
ZnO@g-C ₃ N ₄	Photocatalyst dose of 0.65 g/L, pH 5.6, airflow rate of 1.89 L/min	90.4% oxidative removal within 60 min of reaction time	[20]
Quaternary magnetic BiOCl/g-C ₃ N ₄ /Cu ₂ O/Fe ₃ O ₄ nano-junction	Degradation reaction with catalyst dose of 0.2 g/L, with initial concentration of SMX = 25.328 mg/L, under visible light irradiation (800 W Xenon lamp, with 400 nm cut-off filter)	99.5% degradation under Xenon lamp for irradiation within 1 h and 92.1% degradation under natural sunlight within 2 h	[24]
Fe-Co-O-co-doped g-C ₃ N ₄	-	Complete degradation of 0.04 mM of sulfamethoxazole within 30 min at a reaction rate of 0.085 min ⁻¹	[25]
Se-doped g-C ₃ N ₄	-	93% degradation of SMX in 180 min with a rate constant of 0.0149 min ⁻¹	[27]
g-C ₃ N ₄ /MgO composite	With the dose of the catalyst = 0.2 g/L, initial concentration of SMX = 20 mg/L	92 ± 3% degraded within 3 h	[38]
Heterostructured 2D/2D ZnIn ₂ S ₄ /g-C ₃ N ₄ nanohybrids	In the presence of 0.2 g/L catalyst, initial concentration of SMX = 15 mg/L, under visible light irradiation (solar simulation AM 1.5 G, intensity 100 mW/cm ⁻²)	89.4% degradation in 2 h	[87]
β-CDPs/Fe-g-C ₃ N ₄ catalyst	In the presence of 0.2 g/L catalyst, 2 mM of PMS	Rate constant value of 0.132 min ⁻¹	[88]
FeCo ₂ S ₄ -modified g-C ₃ N ₄ photocatalyst	At a pH of 6.5, a reaction temperature of 40 °C	91.9% degradation with a rate constant of 0.151 min ⁻¹	[89]
Fe-dispersed g-C ₃ N ₄ photocatalyst	Initial concentration of sulfamethoxazole 10 mg/L, dose of catalyst 50 mg/L	98.7% degradation within 6 min	[90]
AgCl/Ag ₃ PO ₄ /g-C ₃ N ₄	With 43% AgCl in the matrix	95% removal within 2 h of reaction time	[91]
Porous g-C ₃ N ₄ modified with ammonium bicarbonate	Under the action of 0.05 g/L catalyst dose, initial concentration of SMX = 0.5 mg/L, at pH 9, under visible light irradiation (150 W Xenon lamp)	93.37% degradation within 30 min	[92]
Ag ₃ PO ₄ /g-C ₃ N ₄	With a catalyst dose of 1 mg/L, under the irradiation of Xenon lamp	Complete degradation within 90 min of visible light irradiation	[93]
Ag/g-C ₃ N ₄	Under the action of 0.05 g/L catalyst dose, 2.538 mg/L of initial concentration of SMX, under the irradiation of Xe lamp (300 W with 400 nm cut-off filter)	99.5% degradation using 10 wt% Ag in the matrix	[94]
g-C ₃ N ₄ nanotubes	Under the action of 0.4 g/L catalyst dose, 100 mg/L of SMX, under irradiation of Xe lamp (300 W)	Complete degradation within 120 min of reaction time	[95]
Porous loofah-sponge-like ternary heterojunction g-C ₃ N ₄ /Bi ₂ WO ₆ /MoS ₂	-	Under visible light irradiation, over 99% degradation took place in 60 min with a rate constant value of 0.089 min ⁻¹	[96]

4.4. Ibuprofen (Ibu)

Ibu is also a nonsteroidal anti-inflammatory drug commonly used for pain relief, fever, and inflammation purposes. In recent years, some studies have been performed on using g-C₃N₄-based catalysts for degrading Ibu from aqueous media. Liu and Tang [97] reported the application of g-C₃N₄/Bi₂WO₆/rGO heterostructured nanocomposite for the degradation of Ibu. Ag/g-C₃N₄/kaolinite composite was applied by Sun et al. [18] for the eradication of Ibu. Mao et al. [98] reported the preparation and application of 1D/2D

nanorod FeV₃O₈/g-C₃N₄ composite catalyst for the degradation of Ibu. In comparison to the g-C₃N₄ nanosheets, the catalytic activity of this nanocomposite was nearly four times higher. The authors proposed a Z-scheme mechanism for the composite. Meng et al. [99] utilized layered g-C₃N₄ and BiOBr photocatalysts for the degradation of Ibu in wastewater. A list is provided in Table 4 regarding the application of various g-C₃N₄-based catalysts towards catalytic eradication of Ibu from water.

Table 4. A list of g-C₃N₄-based catalysts reported for Ibu degradation.

Description of the Catalyst	Reaction Conditions	Optimized Degradation Efficiency	References
Ag/g-C ₃ N ₄ /kaolinite composite	7 wt% Ag, with catalyst dose = 1 g/L, Ibu = 5 mg/L, under visible light irradiation (500 W Xe lamp, with 400 nm filter)	Almost complete degradation in 300 min with, rate constant = 0.0113 min ⁻¹	[18]
g-C ₃ N ₄ /Bi ₂ WO ₆ /rGO heterostructured composites	At a catalyst dose of 0.2 g/L, Ibu concentration = 5 mg/L, pH = 4.3, under visible light irradiation (300 W Xenon lamp with 420 nm filter)	93% degradation with a rate constant of 0.011 min ⁻¹ under visible light irradiation and 98.6% degradation under sunlight	[97]
1D/2D FeV ₃ O ₈ /g-C ₃ N ₄	10 wt% FeV ₃ O ₈ in the matrix, with catalyst dose = 0.33 g/L, Ibu = 10 mg/L, under visible light irradiation (300 W Xenon lamp with 420 nm filter)	95% degradation in 85 min	[98]
Layered g-C ₃ N ₄ and BiOBr	With catalyst dose = 0.2 g/L, Ibu = 20 mg/L	Complete degradation in 10 min	[99]
g-C ₃ N ₄ /Ag/AgCl/BiVO ₄ micro flower composite	Under the catalyst dose of 0.25 g/L, under visible light irradiation (compact fluorescent lamps)	94.7% degradation within 1 h of reaction time	[100]
g-C ₃ N ₄ /MIL-68(In)-NH ₂ heterojunction composite	Under the action of 0.15 g/L of catalyst, 20 mg/L of Ibu concentration, with visible light irradiation (300 W Xenon lamp, with cut-off filter at 420 nm)	Photocatalytic rate = 0.01739 min ⁻¹ , 93% degradation, in 120 min	[101]
TiO ₂ /g-C ₃ N ₄ composite	With catalyst dose of 1 g/L, 5 mg/L of Ibu concentration, under the visible light irradiation (250 W Xe lamp)	Almost complete degradation in 60 min	[102]
TiO ₂ /UV and g-C ₃ N ₄ visible light	With initial concentration of Ibu as 5 mg/L, catalyst dose of 2.69 g/L, at pH 2.51 under the action of 4–10 W LED lamps	Complete degradation in 120 min	[103]
Au-Ag/g-C ₃ N ₄ nanohybrids	With initial concentration of Ibu as 5 mg/L, catalyst dose of 2.69 g/L, under the action of natural sunlight and 4–10 W LED lamps	Complete degradation in 120 min under natural sunlight	[104]
g-C ₃ N ₄ /CQDs/CDIn ₂ S ₄	Initial concentration of Ibu = 80 mg/L, dose of catalyst = 0.1 g/L, under visible light irradiation (300 W Xenon lamp with 420 nm filter)	About 90% degradation in 60 min	[105]
Plasma-treated g-C ₃ N ₄ /TiO ₂	Using g-C ₃ N ₄ /TiO ₂ catalyst with 15 min treatment of plasma oxygen	95% degradation within 90 min	[106]
Triple 2D g-C ₃ N ₄ /Bi ₂ WO ₆ /rGO composites	3 wt% rGO in the composite, catalyst dose = 2 g/L, Ibu = 5 mg/L, pH = 4.3	86% degradation under visible light and 98% removal under natural sunlight	[107]
g-C ₃ N ₄ /Bi ₂ WO ₆ 2D/2D heterojunction	With 0.2 g/L catalyst, initial concentration of Ibu = 103.145 mg/L	96.1% degradation efficiency within 1 h,	[108]
α-SnWO ₄ /UiO-66(NH ₂)/g-C ₃ N ₄ ternary heterojunction	With 0.5 g/L catalyst dose, Ibu = 10 mg/L under visible light irradiation (Xe lamp)	More than 90% degraded in 120 min reaction time	[109]

4.5. Other Drugs

Studies have also been conducted on the application of g-C₃N₄-based catalysts to degrade ciprofloxacin (CIP) from water bodies. Deng et al. [110] reported the preparation and application of Ag-modified phosphorus-doped ultrathin g-C₃N₄/BiVO₄ photocatalyst for the degradation of CIP drug. In the study, more than 92% degradation efficiency was achieved under visible light and near-infrared light irradiation ($\lambda > 420$ nm, $\lambda > 760$ nm), with an initial concentration of CIP 10 mg/L. Zhang et al. [111] applied Fe₃O₄/CdS/g-C₃N₄ composite for the photocatalytic degradation of CIP under visible light irradiation. CdS itself is a photocatalyst. However, the addition of g-C₃N₄ in the composite improved its optical response and the incorporation of Fe₃O₄ nanoparticles helped in the easy recovery of the catalyst. Triclosan (TCS) is a famous nonionic broad-spectrum antimicrobial pharmaceutical compound. However, US Food and Drug Administration banned its usage in 2016 due to the health risk associated with it [112]. In recent years, some research groups also explored g-C₃N₄-based photocatalysts towards triclosan degradation in water. Wang et al. [113] reported the application of g-C₃N₄/MnFe₂O₄ catalyst for the degradation of TCS through PMS activation. The as-prepared catalyst showed promising behavior in terms of stability and metal leaching. Dechlorination, hydroxylation, and cyclization along with other bond-breaking mechanisms were attributed to the triclosan degradation purpose. In one of the recent articles, Yu et al. [114] described the highly efficient degradation performance of a novel catalyst g-C₃N₄/Bi₂MoO₆ towards TCS drug. TCS was converted to 2-phenoxyphenol under visible light irradiation. In 180 min, 95.5% degradation was achieved, which was 3.6 times higher in comparison to that obtained with pure g-C₃N₄ catalyst.

Mafa et al. [115] developed a multi-elemental doped g-C₃N₄ catalyst and tested it towards NPX degradation. Pure g-C₃N₄ catalyst showed poor performance in terms of degradation efficiency (21.5%). With rare earth metals loading (1%), the composite catalyst showed excellent behavior (92.9% efficiency) towards drug removal. A heterojunction was formed between the rare earth metal and the g-C₃N₄ surface which provided the defect for facilitating electron–hole separation. The degradation followed the Z-scheme mechanism with visible light absorption, with the participation of superoxide radicals.

Truong et al. [116] utilized ZnFe₂O₄/BiVO₄/g-C₃N₄ photocatalyst for the efficient removal of lomefloxacin antibiotic degradation. Keeping the amount of ZnFe₂O₄, BiVO₄, and g-C₃N₄ in the ratio 1:8:10, the optimized removal efficiency of 96.1% was obtained after keeping the set-up illuminated for 105 min.

Like the above-mentioned drugs, AMX is another commonly used drug which often occurs in the ecosystem. Mirzaei et al. [117] prepared a magnetic fluorinated mesoporous g-C₃N₄ catalyst for the AMX elimination purpose. Fluorination of the catalyst material provides a facilitating condition for the catalysis by even distribution in the aqueous medium. Due to the inclusion of the iron nanoparticles, the removal efficiency further got enhanced due to the formation of the heterostructure. However, on increasing the iron content, the catalytic efficiency got diminished due to the fact, that the nanoparticles covered the active sites. A list of g-C₃N₄-based catalysts for degrading other PCs is provided in Table 5.

Table 5. A list of g-C₃N₄-based catalysts reported for other PC degradation.

Description of the Catalyst	Target Compound	Optimized Degradation Efficiency	References
g-C ₃ N ₄ /Fe ₃ O ₄ @MIL-100(Fe)	CIP	94.7% degradation of CIP having an initial concentration of 200 mg/L within 120 min of visible light irradiation	[16]
Mesoporous g-C ₃ N ₄	CIP	92.3% degradation with an initial concentration of 4 mg/L, catalyst dose = 1 g/L	[17]

Table 5. Cont.

Description of the Catalyst	Target Compound	Optimized Degradation Efficiency	References
Ag-modified phosphorus-doped ultrathin g-C ₃ N ₄ nanosheets/BiVO ₄ photocatalyst	CIP	92.6% degradation efficiency for CIP with an initial concentration of 10 mg/L	[110]
Fe ₃ O ₄ /CdS/g-C ₃ N ₄	CIP	81% degradation with an initial concentration of CIP = 20 mg/L, catalyst dose = 0.5 g/L in 180 min reaction time	[111]
Lignin nanorods/g-C ₃ N ₄ nanocomposite	TCS	99.9% removal with an initial concentration of TCS = 10 mg/L, catalyst dose = 0.5 g/L in 90 min time	[112]
g-C ₃ N ₄ /MnFe ₂ O ₄	TCS	Almost complete degradation of TCS having initial concentration of 9 mg/L, catalyst dose = 0.2 g/L, in 60 min of reaction time	[113]
g-C ₃ N ₄ /Bi ₂ MoO ₆	TCS	95.5% oxidative removal of TCS (initial concentration = 2 mg/L), catalyst dose = 1 g/L	[114]
Multi-elemental doped g-C ₃ N ₄	NPX	92.9% removal with initial concentration of naproxen = 10 mg/L, catalyst dose = 0.3 g/L	[115]
ZnFe ₂ O ₄ /BiVO ₄ /g-C ₃ N ₄	Lomefloxacin	96.1% removal after 105 min of visible light irradiation, with initial concentration of lomefloxacin = 25 mg/L, with dose of catalyst = 0.5 g/L	[116]
Magnetic fluorinated mesoporous g-C ₃ N ₄	AMX	Initial concentration of AMX 91.35 mg/L, dose of catalyst = 1 g/L, 90% removal	[117]
La/FeO ₃ /g-C ₃ N ₄ /BiFeO ₃	CIP	Almost complete degradation of CIP at initial concentration of 10 mg/L, catalyst dose = 0.4 g/L in 60 min	[118]
S-Ag/TiO ₂ @g-C ₃ N ₄	TCS	92.3% degradation with TCS concentration = 10 mg/L, pH = 7.8, catalyst dose = 0.2 g/L in 60 min	[119]
g-C ₃ N ₄ /NH ₂ -MIL-88B(Fe)	Ofloxacin	96.5% removal in 150 min, with ofloxacin concentration = 10 mg/L, catalyst dose = 0.25 g/L	[120]
Carbon-rich g-C ₃ N ₄ nanosheet	AMX	Complete degradation in 150 min under irradiation of simulated solar light and in 300 min under irradiation of visible light	[121]
SnO ₂ /g-C ₃ N ₄	AMX	92.1% AMX removal in 80 min, with initial concentration of AMX = 10 mg/L, dose of catalyst = 0.25 g/L under 300 W Xe lamp irradiation	[122]

4.6. Application on Multiple Compounds

In some studies, prepared g-C₃N₄-based catalysts have been applied on more than one PC rather than one compound. Dai et al. [123] applied surface hydroxylated g-C₃N₄ nanofibers for the catalytic degradation of TCH, DC, and metoprolol (MT). Within 60 min of reaction time, 97.3%, 88.9%, and 63.2% degradation of TC, DC, and MT, respectively, was achieved. Barium-embedded g-C₃N₄ was tested against CBM and DC degradation [26]. Thang et al. [124] prepared Ag/g-C₃N₄/ZnO nanorods photocatalyst and assigned it for the degradation of commercial drugs, such as paracetamol (PR), cefalexin (CF), and AMX. By applying only a catalyst dose of 0.08 g/L, the degradation of a target compound having a concentration of 40 mg/L was possible. Di et al. [2] applied g-C₃N₄/ZnFeMMO composites for the photocatalytic degradation of Ibu and sulfadiazine (SDZ) drugs. The Z-scheme mechanism was found to be appropriate for the overall process. The degradation of Ibu proceeded via h⁺ generation in the process while OH[•] was responsible for the elimination of SDZ. A list is presented in Table 6, regarding the application of g-C₃N₄-based catalysts for multiple PC degradation.

Table 6. A list of g-C₃N₄-based catalysts reported for multiple PC degradation.

Catalyst	Target Drugs	Optimized Reaction Condition	Reference
g-C ₃ N ₄ /TiO ₂ nanomaterials	PR, Ibu, DC	With an initial concentration of paracetamol = 25 mg/L, Ibu = 15 mg/L, DC = 25 mg/L, catalyst dose = 0.9 g/L, complete degradation of paracetamol and Ibu was possible; however, DC did not get fully degraded	[15]
Single barium-atom-embedded g-C ₃ N ₄ catalyst	DC and CBM	Almost complete degradation of CBZ (1 mg/L) and DC (8 mg/L) under visible light irradiation in 60 min	[26]
α-Fe ₂ O ₃ /g-C ₃ N ₄	CFX and AMX	Complete degradation of both drugs at initial concentration of 20 mg/L within 180 min	[31]
Carbon quantum dots modified reduced ultrathin g-C ₃ N ₄	DC, TCS, NPX	100% degradation within 6 min	[80]
Carbon-doped supramolecule-based g-C ₃ N ₄ /TiO ₂ composites	DC and CBM	98.92% and 99.77% degradation of DC and CBZ in 30 min and 6 h illumination under LED	[81]
0D/1D Co ₃ O ₄ quantum dots/surface-hydroxylated g-C ₃ N ₄ nanofibers	TC, DC, MT	97.3% degradation for TC, 88.9% for DC, 63.2% for MT in 60 min of reaction time	[123]
Ag/g-C ₃ N ₄ /ZnO nanocomposite	PR, AMX, CFX	With an initial concentration of each drug = 40 mg/L, catalyst dose = 0.08 g/L, 78% degradation for PR, 70% for cefalexin, and 35% for AMX	[124]
g-C ₃ N ₄ -supported WO ₃ /BiOCl heterojunction	LFX and TCH	92.5% degradation of TCH at initial concentration of 20 mg/L	[125]
(2D/3D/2D) rGO/Fe ₂ O ₃ /g-C ₃ N ₄ nanostructure	TC and CIP	Complete degradation of both compounds at an initial concentration of 50 mg/L within 60 min	[126]

5. Optimization Techniques

Optimization of the photocatalyst is one of the pertinent areas for proper resource utilization. In the present era, multiparameter optimization has gained more predominance in comparison to single-parameter optimization. Response surface methodology (RSM) and artificial neural network (ANN) are commonly used for this purpose. Mirzaei et al. [20] used the RSM technique for the photodegradation of SMX by taking catalyst dose, solution pH, and airflow rate as the variables. The authors used central composite design (CCD) for RSM analysis and the catalyst dose, pH, and airflow rate were varied in the range of 0.4–0.8 g/L, 3–11, and 0.5–2.5 L/min, respectively. Twenty experiments were run for the purpose and the experimental values showed a good correlation with the predicted values ($R^2 = 0.9802$). The optimum condition was found as 0.65 g/L of photocatalyst dose, pH of 5.6, and airflow rate of 1.89 L/min and under this condition, the removal efficiency achieved was 94%. Shanavas et al. [126] conducted an optimization study regarding the application of rGO-gC₃N₄-based catalysts for TC and CIP degradation. The reaction time, reaction temperature, and molar concentration were chosen as the variables for the purpose.

John et al. [82] explored RSM for the optimization of DC degradation. Four variables, namely, irradiation time, initial solution pH, initial DC concentration, and g-C₃N₄ loading, were chosen for the study. From the analysis, it was found that the optimum reaction conditions were obtained as irradiation time = 90 min, initial solution pH = 5, initial DC concentration = 5 ppm, and g-C₃N₄ loading = 0.3 g/g TiO₂, and the maximum removal efficiency achieved was 93.49%.

Quarajehdaghi et al. [127] optimized photocatalytic degradation of CIP by application of CdS/g-C₃N₄/rGO/CMC catalyst using RSM and ANN approach. Four parameters were chosen for the RSM study, such as initial concentration of CIP, dose of catalyst, pH, and time

of irradiation. Using the CCD model, 30 experiments were run. Predicted removal efficiency shows a good correlation with the experimental values. The quadratic model best fitted the trend with a high R^2 value of 0.9827. From the RSM analysis, the condition for the optimized removal efficiency was determined as initial concentration of CIP = 7.89 mg/L, the dose of catalyst = 0.6 g/L, pH = 6.15, and irradiation time = 33.94 min. The predicted optimized removal was 84.25%, while experimentally, the removal was achieved at 81.93%. From the ANN study, the relative importance of different parameters on the degradation efficiency was determined. It was seen that the influence of the dose of catalyst was the highest (34%), followed by pH (30%), irradiation time (26%), and, lastly, initial concentration of CIP (10%). Furthermore, the values obtained from the ANN model were also compared with those obtained from the RSM model as well as with the experimental values. The values found from RSM, ANN, and experimental investigation were quite close to each other.

AttariKhasraghi et al. [128] also used RSM and ANN models for cefoperazone degradation using a zeolite-supported CdS/g-C₃N₄ catalyst. CCD model was used for the purpose using four variables, such as dose of catalyst, initial concentration of cefoperazone, pH, and time. The degradation percentages predicted by both the models (RSM and ANN) showed a good correlation with the experimentally obtained values. Using RSM analysis, the optimized condition was found as the dose of catalyst = 0.4 g/L, initial concentration of cefoperazone = 17 mg/L, pH = 9, and time = 80 min. The predicted maximum removal efficiency was 95.66%, while actually 93.23% was achieved. It proves the accuracy of the model.

6. Real Field Application

It is pertinent to check the performance of the catalyst towards real wastewater. For utilization of the novel g-C₃N₄-based catalyst in real wastewater treatment, firstly scaling up the process is mandatory. Plasma reactor is one of the innovative reactors which has the feasibility of being applied in the real field scenario. Feyzi et al. [19] used ZnO/g-C₃N₄/zeolite-P-supported catalyst in a dielectric barrier discharge plasma reactor for photodegradation of TC.

Kumar et al. [129] reported the application of novel g-C₃N₄/TiO₂/Fe₃O₄@SiO₂ photocatalyst for the degradation of Ibu in sewage. Ibu concentration was kept at 2 mg/L, while the dose of the photocatalyst was maintained at 1 g/L and 2 g/L. With a 1 g/L dose of catalyst, only 13% degradation efficiency was achieved, while with a 2 g/L dose, 92% efficiency was obtained. Nivetha et al. [122] tested the potency of the SnO₂/g-C₃N₄ nanocomposite photocatalyst towards the degradation of real pharmaceutical effluent after being successful towards degrading AMX. Untreated pharmaceutical effluent shows a strong absorbance at 280 nm. However, after the application of the novel photocatalyst, the peak started decreasing with the fading of the solution visible to the naked eye.

Rapti et al. [130] investigated the photocatalytic efficiency of g-C₃N₄ and 1% MoS₂/g-C₃N₄ catalysts towards 10 psychiatric drugs in hospital wastewater effluent. Experiments were conducted in a stainless-steel lamp reactor of volume 46 L provided with 10 UVA lamps and quartz filters connected to a propylene recirculation tank of volume 55–100 L. The composite catalyst (1% MoS₂/g-C₃N₄) showed higher catalytic performance compared to that obtained with pure g-C₃N₄ catalyst. The degradation efficiency for every pharmaceutical compound varies in the range of 91–100%. Moreover, the reaction was also conducted in a solar simulator under the irradiation of 500 Wm⁻², where the degradation efficiency was maintained in the range of 54–100%. Further, the study was escalated to the pilot wastewater treatment plant (parabolic reactor) established at University Hospital, Ioannina City. The degradation efficiency of the targeted pharmaceutical compounds was evaluated using natural sunlight as the source of irradiation. All the samples were analyzed using solid phase extraction followed by chromatographic measurements. Antonopoulou et al. [131] used a g-C₃N₄ catalyst under the irradiation of UVA light for the catalytic degradation of amisulpride, a psychiatric drug in distilled water as well as in municipal wastewater. High degradation percentage was maintained in both the distilled water and

municipal wastewater matrix. However, a slower reaction rate was observed in the case of the latter due to the complex nature of the real wastewater.

Kumar et al. [132] developed a novel g-C₃N₄ nanorod catalyst by hydrothermal method. Thus, the prepared activated g-C₃N₄ catalyst exhibited higher degradation efficiency in comparison to that of the bare g-C₃N₄ material. The catalytic efficiency was tested towards 17 α -ethinylestradiol in real hospital wastewater effluent. Within 45 min of reaction time, high removal percentage was attained.

Jin et al. [80] applied the as-prepared quantum carbon dot modified g-C₃N₄ photocatalyst for the oxidative degradation of DC in distilled water as well as DC spiked in tap water, wastewater treatment plant effluent, Pearl River water, lake water, and South China Sea water. In comparison to the distilled water, degradation efficiency got reduced in the range of 5–13% for different real water matrices. The reduction in removal efficiency might have caused due to the presence of several that act as light filters and electron trappers. Further investigation on the interference study revealed that certain anions such as chloride, sulfate, and nitrate had minimal adverse effects on the degradation efficiency. However, the presence of HCO₃[−] caused a moderate hindrance to the reaction as it can quench OH[·] to form less reactive CO₃^{2−}. In the presence of Cu²⁺ and Fe³⁺, removal efficiency got reduced significantly, as it reacted with O₂^{·−} prior to the degradation of DC.

7. Characterization Techniques

7.1. Fourier Transformed Infrared Spectroscopy (FTIR)

FTIR analysis is a common tool for knowing the functional groups involved in the degradation process. In the work of Kumar et al. [132], strong peaks were noticed around 1515 cm^{−1} corresponding to the C-N= stretching vibration. The appearances of a double peak at 1276 and 1350 cm^{−1} are designated to the aromatic C-N stretching. In the photocatalytic degradation study of DC by reduced ultrathin g-C₃N₄ decorated with quantum carbon dots, FTIR spectra of ultrathin carbon nitride (UCN), reduced ultrathin carbon nitride (RUCN), and carbon quantum dots decorated ultrathin g-C₃N₄ were recorded [80]. In all the spectra, peaks appeared at 810 cm^{−1}, 1200–1700 cm^{−1}, and 3000–3700 cm^{−1} corresponding to the bending mode of triazine units, stretching vibration due to C-N heterocycles, and N-H vibrations, respectively.

7.2. Electron Microscopic Analysis

Morphological features of the g-C₃N₄ catalyst are obtained from electron microscopic analysis, such as scanning electron microscopy (SEM) and transmission electron microscopy (TEM). Mafa et al. [115] conducted both SEM and TEM analyses of the different elements (Ce, Er, Gd, and Sm) doped g-C₃N₄ catalysts. The pure g-C₃N₄ catalyst exhibits a tubular structure with small openings. Due to doping, the tubular structure got transformed to flake-like structure. Cerium doping reduces the size of the flake. The SEM image is shown in Figure 7.

In another study, Palanivel et al. found from the SEM image that the structure of S-doped g-C₃N₄ resembled to that of the nanorods [47]. On the other hand, NiFe₂O₄ nanoparticles possessed agglomerating structure. The nanorod structure helped in improving charge carrier mobility and facilitated electron channelization which ultimately made the composite a suitable photocatalyst. In the work of Peng et al. [88], the 3D porous structure of β CDPs/Fe-g-C₃N₄ catalyst was confirmed by both SEM and TEM analyses.

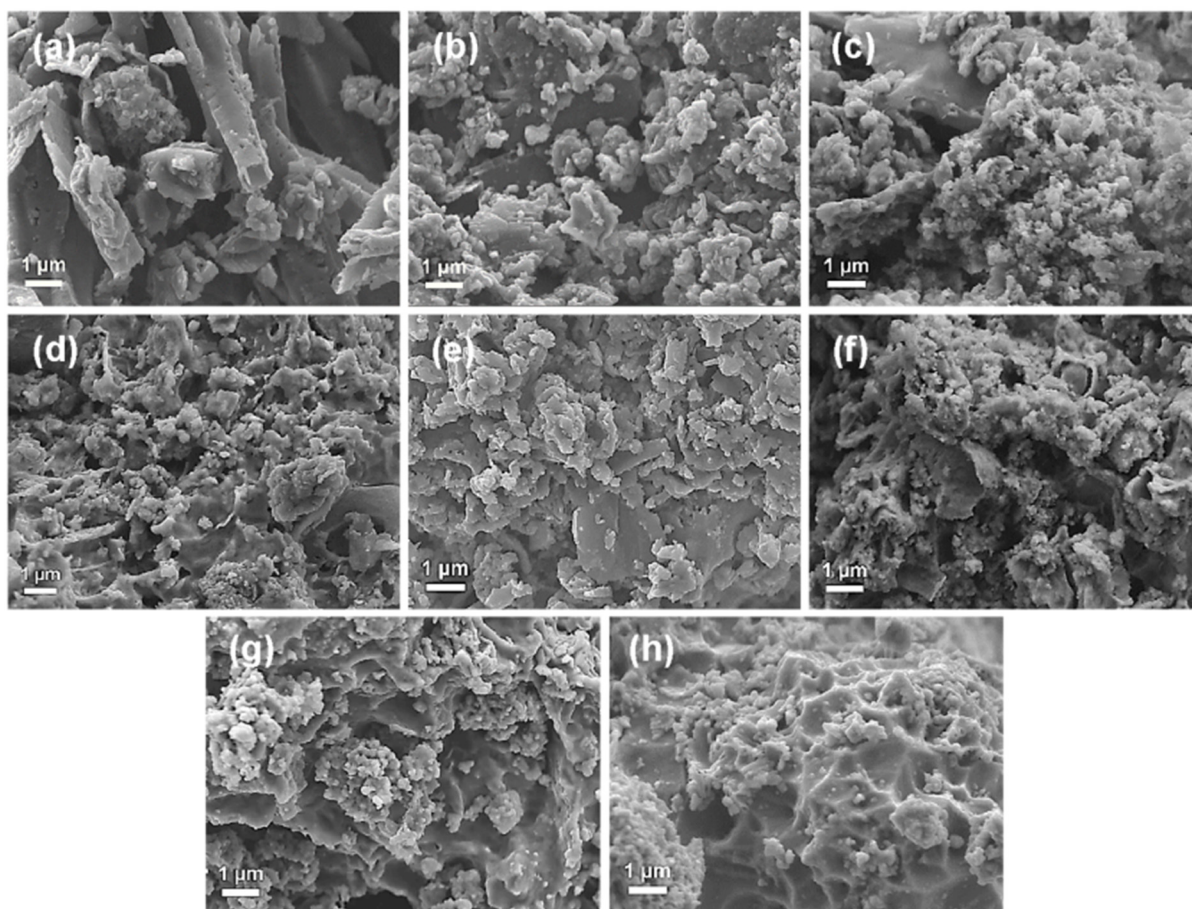


Figure 7. FESEM micrograms of (a) CN, (b) CeCN, (c) ErCN, (d) GdCN, (e) SmCN, (f) 1RECN, (g) 3RECN, and (h) 5RECN photocatalysts [115].

7.3. BET Surface Area Analysis

BET surface area analysis is important for providing insight into the porosity and surface area of the catalyst material. Mirzaei et al. [117] found the specific surface area of the prepared fluorinated $g\text{-C}_3\text{N}_4$ catalyst as $\sim 243 \text{ m}^2/\text{g}$. On the other hand, the specific surface area of bare $g\text{-C}_3\text{N}_4$ was found to be around $37.85 \text{ m}^2/\text{g}$. Enhancement in the specific surface area of the $g\text{-C}_3\text{N}_4$ nanosheets occurred due to the acid-assisted hydrothermal treatment. The pore volume of the bare $g\text{-C}_3\text{N}_4$ and fluorinated catalyst was $0.082 \text{ cm}^3/\text{g}$ and $0.427 \text{ cm}^3/\text{g}$, respectively. The nitrogen adsorption–desorption isotherm showed a similar trend with the type IV isotherm.

In the study of TC degradation by Ba-doped $g\text{-C}_3\text{N}_4$ catalyst, BET surface area analysis for $g\text{-C}_3\text{N}_4$ and the composite material was performed [49]. Pure $g\text{-C}_3\text{N}_4$ had a specific surface area of $9.98 \text{ m}^2/\text{g}$. On the other hand, due to the composite formation, it got increased to $11.41 \text{ m}^2/\text{g}$. Similar results were also found in the case of pore volume measurements ($0.068 \text{ m}^3/\text{g}$ for $g\text{-C}_3\text{N}_4$ and $0.073 \text{ m}^3/\text{g}$ for the composite).

7.4. XPS Analysis

The chemical composition of the constructed photocatalyst and the oxidation states of the elements involved are obtained from the XPS analysis. Guo et al. [12] performed the XPS analysis of a 5% $\text{Cu}_3\text{P-ZSO-CN}$ catalyst. The survey spectra revealed the presence of the Zn 2p, Sn 3d, O 1s, P 2p, Cu 3d, C 1s, and N 1s, and no impurities were found in the catalyst. Furthermore, the high-resolution spectra of Zn 2p displayed strong peaks appearing at 1021.5 eV and 1044.8 eV corresponding to Zn $2p_{3/2}$ and Zn $2p_{1/2}$. In Sn 3d spectrum, peaks appeared at 486.4 eV and 494.7 eV denoting the presence of Sn $3d_{5/2}$ and

Sn 3d_{3/2}. Chen et al. [102] performed the XPS analysis of TiO₂, g-C₃N₄, and TiO₂/g-C₃N₄ (5% weight) in order to get an idea regarding the surface chemical properties.

Liang et al. [96] conducted the XPS analysis in order to get a clear idea regarding the elemental composition as well as the surface chemical properties of the composite catalyst. From the survey spectrum, prominent peaks of the elements C, N, O, Mo, and Bi were visible. No signal corresponding to S and W was noticeable, which might be due to their presence in very low concentrations. In the O1s spectrum, peaks corresponding to W-O and Bi-O at 232.7 eV and 229.9 eV were visible. On the other hand, Mo 3d peaks at 232.7 eV and 229.9 eV, corresponding to Mo 3d_{3/2} and Mo 3d_{5/2}, implying that Mo is in a +4 state, were observed. The XPS spectra are shown in Figure 8.

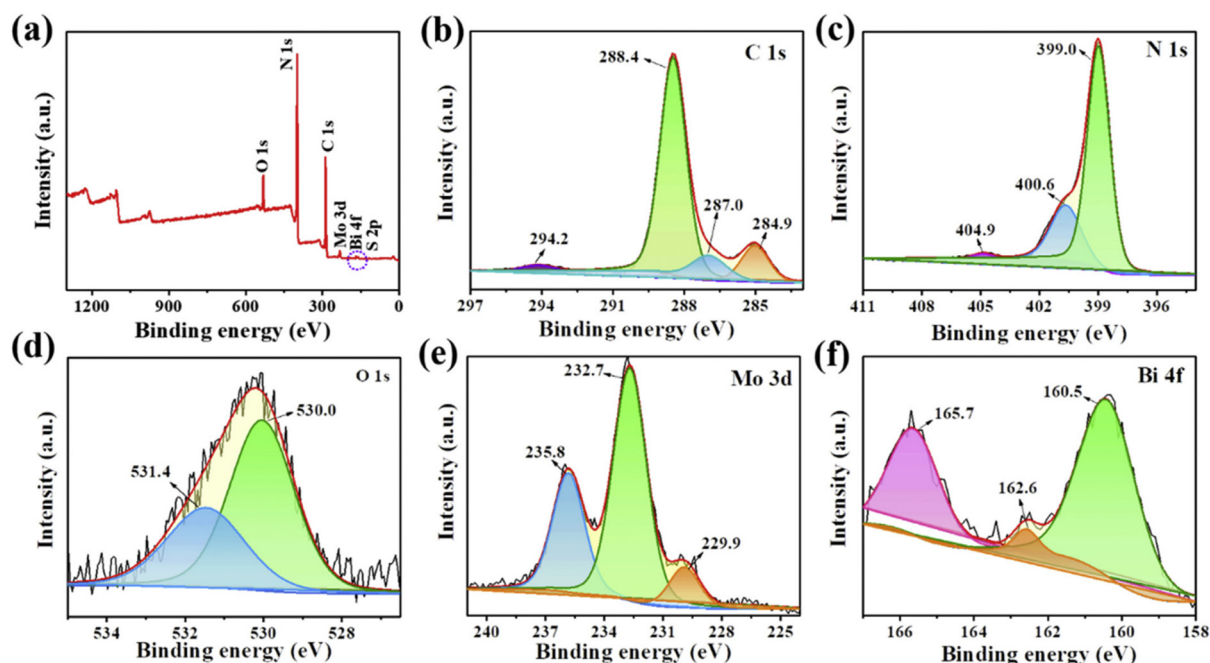


Figure 8. XPS of (a) survey spectra, (b) C 1s, (c) N 1s, (d) O 1s, (e) Mo 3d, and (f) Bi 4f of CN-BM2 [96].

Kumar et al. [129] conducted an XPS analysis of the g-C₃N₄/TiO₂/Fe₃O₄@SiO₂ (gCTFS) catalyst. The wide-scan spectra indicated that the nano photocatalyst was composed of Fe, Si, Ti, C, N, and O. Among all these elements, the signal corresponding to N was very weak indicating that only a few nitrogen atoms were retained after calcination.

7.5. Diffuse Reflectance Spectra (DRS) Analysis

Optical features of the as-synthesized photocatalysts are often explored by conducting diffuse reflectance spectral (DRS) analysis. Baladi et al. [21] performed the DRS analysis of the pure g-C₃N₄, ZnO, and the composite prepared from both. The absorption edges for g-C₃N₄ and ZnO appeared at 445 nm and 405 nm corresponding to the bandgap of 2.78 eV and 3.1 eV. However, after forming the composite, a redshift in comparison to the ZnO appeared indicating a better electron–hole separation efficiency, and an enhanced visible light absorption by the composite photocatalyst. Moreover, the absorption intensity for the composite got increased with respect to the pure g-C₃N₄ indicating the presence of ZnO in the matrix.

Jin et al. [80] carried out the UV-vis DRS analysis of the as-prepared ultrathin g-C₃N₄ photocatalysts. Ultrathin g-C₃N₄ (UCN) showed a strong absorption edge at 460 nm while in the case of reduced UCN, the absorption edge showed a red shift due to the nitrogen defects. Moreover, due to the carbon quantum dot modification, it was shifted to 480 nm which indicates that the incorporation of CQD can enhance the spectral response.

Palanivel et al. [47] found that the absorption of bare g-C₃N₄ occurred at 467 nm with a bandgap of 2.65 eV. On the other hand, carbon nitride nanorod (CNNR) material shows strong absorption at 452 nm. It happened due to the quantum confinement effect. During the formation of the nanocomposite, its electronic state became discrete and hence a blue shift is observed in comparison to the bulk parent material. Moreover, due to sulfur doping, SCNNR showed a strong absorption at 479 nm with a bandgap of 2.58 eV. Due to the incorporation of the S atom, the band gap is shortened.

7.6. X-ray Diffraction (XRD) Analysis

XRD analysis is often explored by researchers for finding out the size of the photocatalyst material. It is based on the Debye–Scherer equation as follows:

$$d = \frac{0.9\lambda}{\beta \cos \theta} \quad (1)$$

Di et al. [2] performed the XRD analysis of g-C₃N₄/ZnMMO composite catalyst. In the XRD spectra of pure g-C₃N₄, two prominent peaks were observed at 13.2° and 27.4°. It refers to the (100) and (002) planes, respectively, which indicates interplanar repeated packing of tri-s-triazine rings and interlayer stacking of graphitic-like structure. In the XRD spectrum of ZnFeMMO, diffraction peaks corresponding to hexagonal wurtzite ZnO and ZnFe₂O₄ were clearly observed. On the other hand, after the formation of the composite between the two, the peaks got diminished in magnitude indicating a strong interaction between the two.

Kumar et al. [129] carried out the XRD analysis of Fe₃O₄, Fe₃O₄@SiO₂, g-C₃N₄ nanosheets, and the composite catalyst with TiO₂. In the spectrum of Fe₃O₄, five peaks at 30.1°, 35.5°, 43.1°, 57°, and 62.6° were observed corresponding to (220), (311), (400), (511), and (440) planes. However, in Fe₃O₄@SiO₂, after forming a composite with SiO₂, no characteristic peak due to SiO₂ was observed. Finally, in the spectrum of the composite catalyst (g-C₃N₄/TiO₂/Fe₃O₄@SiO₂), peaks were found at 25.4°, 38°, 48°, 53.9°, 55.19°, 62.72°, 69°, 70.25°, and 75.3° corresponding to the TiO₂.

7.7. Photoluminescence (PL) Spectroscopy

PL spectra are often explored by research groups to have more insight into the photocatalytic property of as-synthesized composite materials. Yan et al. [133] recorded the PL spectra of the pristine g-C₃N₄ material as well as the metal (Na, K, Ca, Mg) doped g-C₃N₄ matrix. A strong absorption peak around 440 nm is observed for the pure g-C₃N₄ while similar spectra with reduced intensity are being observed for the doped materials (as shown in Figure 9). Reduction in the PL intensity indicates that the electron–hole recombination is reduced as well as the lifetime of the charge carrier is increased. Mirzaei et al. [117] reported that due to the fluorination of the g-C₃N₄ catalyst, the intensity of the photoluminescence spectra got reduced.

7.8. Identification of the Intermediate Products

In pharmaceutical degradation, the identification of the intermediate products constitutes an important study. In the photocatalytic degradation of Ibu by g-C₃N₄/TiO₂/Fe₃O₄@SiO₂ photocatalyst, the intermediate compounds were identified [129]. Peaks were obtained at *m/z* 237, 253, 241, 257, 165, and 163 as a result of the hydroxylation, decarboxylation, and demethylation. Moreover, according to the mass balance equation, 6.5 μmol of CO₂ was obtained after the complete mineralization of 10 μmol of Ibu.

Huang et al. [134] identified the intermediate products by LC-MS analysis while degrading CBZ by a g-C₃N₄ heterogeneous catalyst through the Fenton process. A prominent peak was identified corresponding to an *m/z* ratio of 253 due to hydroxyl substitution reaction. During the reaction process, a loss of CONH₂ occurred which was reflected by the strong signal at the *m/z* value of 193.

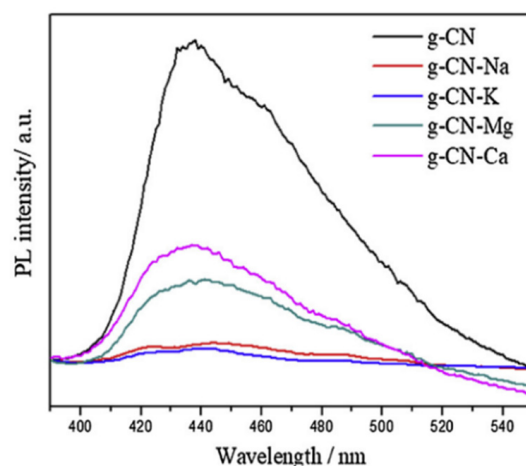


Figure 9. PL spectra of pristine and doped $g\text{-C}_3\text{N}_4$ samples [133].

7.9. Photoelectrochemical Tests

Photoelectrochemical tests constitute an important characterization of the photocatalyst material as it gives insight into the charge transfer mechanism of the synthesized material. Guo et al. [14] showed that in comparison to the bare $g\text{-C}_3\text{N}_4$ catalyst, the Cl-doped catalyst revealed higher photocurrent density which implied that the electron–hole recombination could be prevented more effectively due to Cl doping. He et al. [4] carried out the photoelectrochemical test of the $\text{Ti}_3\text{C}_2/g\text{-C}_3\text{N}_4$ photocatalyst using Na_2SO_4 as the electrolyte. It was seen that the photocurrent response of the $\text{Ti}_3\text{C}_2/g\text{-C}_3\text{N}_4$ catalyst was higher in comparison to the bare $g\text{-C}_3\text{N}_4$ material. Due to the high conductivity of Ti_3C_2 , photo-generated electrons from the surface of $g\text{-C}_3\text{N}_4$ got transported to the Ti_3C_2 surface resulting in high charge separation and greater photocurrent response. Furthermore, the Nyquist plot revealed that the impedance value of $\text{Ti}_3\text{C}_2/g\text{-C}_3\text{N}_4$ is lower than that of $g\text{-C}_3\text{N}_4$, which indicates the efficient generation of photoelectrons under visible light irradiation. Moreover, it also confirmed the 2D/2D nanostructure of the newly synthesized catalyst.

7.10. Electron Spin Resonance (ESR) Tests

The ESR technique is often explored by researchers to investigate the reactive oxygen species (ROS) involved in the degradation process. Chen et al. [30] used 5,5-dimethyl-1-pyrroline N-oxide (DMPO) as a spin-trap chemical in the aqueous dispersion of methanol. Results showed peaks of both $\text{DMPO}\cdot\text{O}_2^-$ and $\text{DMPO}\cdot\text{OH}$ adducts appeared in the ESR spectrum. Hence, it can be concluded that under visible light irradiation, the Mn/SCN-20 photocatalyst was able to generate both superoxide and hydroxyl radicals to facilitate TC degradation. Cao et al. [51] utilized DMPO for trapping and detecting radicals such as $\cdot\text{OH}$, $\cdot\text{O}_2^-$, and $\text{SO}_4^{\cdot-}$ generated during the catalytic degradation of TCH, while 2,2,6,6-tetramethylpiperidine-1-oxyl for the detection of $^1\text{O}_2$ radical. The results showed that the 4%P/CNK catalyst was efficient to generate $\cdot\text{OH}$, $\cdot\text{O}_2^-$, $\text{SO}_4^{\cdot-}$, and $^1\text{O}_2$ radicals for TCH degradation purposes under the combined action of visible light irradiation and PMS.

8. Future Perspective and Current Challenges

$g\text{-C}_3\text{N}_4$ -based photocatalysts are undoubtedly promising materials for pharmaceutical wastewater treatment. Scientists are rigorously working in this field for further development of newer catalysts and their applicability for real field applications. In spite of various achievements, there still exist several challenges and hurdles which need to be overcome. Production of a highly stable $g\text{-C}_3\text{N}_4$ -based photocatalyst with a narrow band gap is still a challenging task. More control over the surface defects and other properties has to be attained through rigorous research. Another aspect is the synthesis cost of $g\text{-C}_3\text{N}_4$ -based catalysts causing the major hurdle behind their large-scale applications.

Balakrishnan et al. [7] in their recent review article highlighted serious challenges associated with the usage of $g\text{-C}_3\text{N}_4$ catalysts for environmental remediation purposes. One of the major problems associated with the $g\text{-C}_3\text{N}_4$ -based catalysts is the high electron–hole recombination and significant loss of weight while reusing the catalyst as already mentioned in the introduction part. To improve light absorption, scientists are continuously developing novel techniques for reducing bandgap. Several reports on $g\text{-C}_3\text{N}_4$ showed a significant reduction in band gap that occurred due to the modification or immobilization. However, a detailed explanation behind this bandgap reduction is often not dealt with. Hayat et al. [135] also commented that the charge transfer mechanism of the $g\text{-C}_3\text{N}_4$ -based catalysts is not always fully understood. Hence, a more rigorous effort is recommended.

Many $g\text{-C}_3\text{N}_4$ -based catalysts have been proven to be toxic to the aquatic ecosystem. Hence, toxicity analysis should also be dealt with while applying these materials for pharmaceutical wastewater treatment.

Often magnetic catalysts are designed for various types of pollutant elimination. However, using a simple bar magnet may lead to severe weight loss during recyclability. Hence, proper design in this respect should be adopted.

$g\text{-C}_3\text{N}_4$ -based photocatalytic membranes are often explored by researchers for pollutant degradation purposes. Fouling and low mass transfer issues often hinder their use in large-scale industrial purposes. In this respect, uncommon ceramic materials can be explored for the optimization of the cost.

Doping is often tried out to enhance the photocatalytic activity of the $g\text{-C}_3\text{N}_4$ -based catalysts. Patnaik et al. [136], in their recent review article, mentioned that in many cases doped $g\text{-C}_3\text{N}_4$ -based catalysts showed poor stability under extreme thermal conditions. Moreover, dopant atoms often become the new area for recombination. Hence, co-doping has been suggested by the authors rather than single-element doping. Although many studies are reported in the literature, still more research is required for controlled doping in order to produce the optimized catalyst.

Yuda and Kumar [137] highlighted some of the important limitations of using $g\text{-C}_3\text{N}_4$ -based catalysts for real-field wastewater systems. Firstly, their stability under different environmental conditions is not often explored. Hence, stability against acidic conditions, temperature variation, etc., should be checked. Moreover, electron–hole separation can be easily understood in two-component heterostructure systems. However, it becomes complicated in the case of multicomponent systems.

Author Contributions: S.B.: Writing, original draft preparation, A.P.: Writing, reviewing. All authors have read and agreed to the published version of the manuscript.

Funding: This research received no external funding.

Data Availability Statement: No new data is created.

Conflicts of Interest: The authors declare no conflict of interest.

Abbreviations

AMX	amoxicillin
ANN	artificial neural network
CBZ	carbamazepine
CFX	cefalexin
CIP	ciprofloxacin
DC	diclofenac
LFX	levofloxacin
NPX	naproxen
OTC	oxytetracycline
PC	pharmaceutical compound
PMS	peroxymonosulfate

PRRSM	paracetamol response surface methodology
SDZ	sulfadiazine
SMX	sulfamethoxazole
TC	tetracycline
TCH	tetracycline hydrochloride
TCS	triclosan

References

- Mahamallik, P.; Saha, S.; Pal, A. Tetracycline degradation in aquatic environment by highly porous MnO₂ nanosheet assembly. *Chem. Eng. J.* **2015**, *276*, 155–165. [[CrossRef](#)]
- Di, G.; Zhu, Z.; Huang, Q.; Zhang, H.; Zhu, J.; Qiu, Y.; Yin, D.; Zhao, J. Targeted modulation of g-C₃N₄ photocatalytic performance for pharmaceutical pollutants in water using ZnFe-LDH derived mixed metal oxides: Structure-activity and mechanism. *Sci. Total Environ.* **2019**, *650*, 1112–1121. [[CrossRef](#)] [[PubMed](#)]
- Nguyen, M.D.; Nguyen, T.B.; Tran, L.H.; Nguyen, T.G.; Fatimah, I.; Kuncoro, E.P.; Doong, R. Z-scheme S, B co-doped g-C₃N₄ nanotube@MnO₂ heterojunction with visible-light-responsive for enhanced photodegradation of diclofenac by peroxy monosulfate activation. *Chem. Eng. J.* **2023**, *452*, 139249. [[CrossRef](#)]
- He, J.; Yang, J.; Jiang, F.; Liu, P.; Zhu, M. Photo-assisted peroxy monosulfate activation via 2D/2D heterostructure of Ti₃C₂/g-C₃N₄ for degradation of diclofenac. *Chemosphere* **2020**, *258*, 127339. [[CrossRef](#)]
- Morales-Paredes, C.A.; Rodriguez-Diaz, J.M.; Boluda-Botella, N. Pharmaceutical compounds used in the COVID-19 pandemic: A review of their presence in water and treatment techniques for their elimination. *Sci. Total Environ.* **2022**, *814*, 152691. [[CrossRef](#)]
- Pattanayak, D.S.; Pal, D.; Mishra, J.; Thakur, C. Noble metal-free doped graphitic carbon nitride (g-C₃N₄) for efficient photodegradation of antibiotics: Progress, limitations, and future directions. *Environ. Sci. Pollut. Res.* **2023**, *30*, 25546–25558. [[CrossRef](#)]
- Balakrishnan, A.; Chinthala, M.; Polagani, R.K.; Vo, D.N. Removal of tetracycline from wastewater using g-C₃N₄ based photocatalysts: A review. *Environ. Res.* **2023**, *216*, 114660. [[CrossRef](#)]
- Ghosh, U.; Pal, A. Insight into the multiple roles of nitrogen doped carbon quantum dots in an ultrathin 2D-0D-2D all-solid-state Z scheme heterostructure and its performance in tetracycline degradation under LED illumination. *Chem. Eng. J.* **2022**, *431*, 133914. [[CrossRef](#)]
- Ghosh, U.; Majumdar, A.; Pal, A. 3D macroporous architecture of self-assembled defect engineered ultrathin g-C₃N₄ nanosheets for tetracycline degradation under LED light irradiation. *Mater. Res. Bull.* **2021**, *133*, 111074. [[CrossRef](#)]
- Ghosh, U.; Pal, A. Drastically enhanced tetracycline degradation performance of a porous 2D g-C₃N₄ nanosheet photocatalyst in real water matrix: Influencing factors and mechanism insight. *J. Water Process Eng.* **2022**, *50*, 103315. [[CrossRef](#)]
- Majumdar, A.; Ghosh, U.; Pal, A. Novel 2D/2D g-C₃N₄/Bi₄NbO₈Cl nano-composite for enhanced photocatalytic degradation of oxytetracycline under visible LED light irradiation. *J. Colloid Interface Sci.* **2021**, *584*, 320–331. [[CrossRef](#)]
- Guo, F.; Huang, X.; Chen, Z.; Cao, L.; Cheng, X.; Chen, L.; Shi, W. Construction of Cu₃P-ZnSnO₃-g-C₃N₄ p-n-n heterojunction with multiple built-in electric fields for effectively boosting visible-light photocatalytic degradation of broad-spectrum antibiotics. *Sep. Purif. Technol.* **2021**, *265*, 118477. [[CrossRef](#)]
- Chi, X.; Liu, F.; Gao, Y.; Song, J.; Guan, R.; Yuan, H. An efficient B/Na co-doped porous g-C₃N₄ nanosheets photocatalyst with enhanced photocatalytic hydrogen evolution and degradation of tetracycline under visible light. *Appl. Surf. Sci.* **2022**, *576*, 151837. [[CrossRef](#)]
- Guo, F.; Li, M.; Ren, H.; Huang, X.; Shu, K.; Shi, W.; Lu, C. Facile bottom-up preparation of Cl-doped porous g-C₃N₄ nanosheets for enhanced photocatalytic degradation of tetracycline under visible light. *Sep. Purif. Technol.* **2019**, *228*, 115770. [[CrossRef](#)]
- Smykalova, A.; Sokolova, B.; Foniok, K.; Matejka, V.; Praus, P. Photocatalytic degradation of selected pharmaceuticals using g-C₃N₄ and TiO₂ nanomaterials. *Nanomaterials* **2019**, *9*, 1194. [[CrossRef](#)] [[PubMed](#)]
- He, W.; Jia, H.; Li, Z.; Miao, C.; Lu, R.; Zhang, S.; Zhang, Z. Magnetic recyclable g-C₃N₄/Fe₃O₄@MIL-100(Fe) ternary catalyst for photo-Fenton degradation of ciprofloxacin. *J. Environ. Chem. Eng.* **2022**, *10*, 108698. [[CrossRef](#)]
- Wang, F.; Feng, Y.; Chen, P.; Wang, Y.; Su, Y.; Zhang, Q.; Zeng, Y.; Xie, Z.; Liu, H.; Liu, Y.; et al. Photocatalytic degradation of fluoroquinolone antibiotics using ordered mesoporous g-C₃N₄ under simulated sunlight irradiation: Kinetics, mechanism, and antibacterial activity elimination. *Appl. Catal. B Environ.* **2018**, *227*, 114–122. [[CrossRef](#)]
- Sun, Z.; Zhang, X.; Dong, X.; Liu, X.; Tan, Y.; Yuan, F.; Zheng, S.; Li, C. Hierarchical assembly of highly efficient visible-light-driven Ag/g-C₃N₄/kaolinite composite photocatalyst for the degradation of ibuprofen. *J. Mater.* **2020**, *6*, 582–592. [[CrossRef](#)]
- Feyzi, L.; Rahemi, N.; Allahyari, S. Efficient degradation of tetracycline in aqueous solution using a coupled S-scheme ZnO/g-C₃N₄/zeolite P supported catalyst with water falling film plasma reactor. *Process Saf. Environ. Prot.* **2022**, *161*, 827–847. [[CrossRef](#)]
- Mirzaei, A.; Yerushalmi, L.; Chen, Z.; Haghghat, F. Photocatalytic degradation of sulfamethoxazole by hierarchical magnetic ZnO@g-C₃N₄: RSM optimization, kinetic study, reaction pathway and toxicity evaluation. *J. Hazard. Mater.* **2018**, *359*, 516–526. [[CrossRef](#)]

21. Baladi, E.; Davar, F.; Hojjati-Najafabadi, A. Synthesis and characterization of g-C₃N₄-CoFe₂O₄-ZnO magnetic nanocomposites for enhancing photocatalytic activity with visible light for degradation of penicillin G antibiotic. *Environ. Res.* **2022**, *215*, 114270. [[CrossRef](#)] [[PubMed](#)]
22. Chen, D.; Li, B.; Pu, Q.; Chen, X.; Wen, G.; Li, Z. Preparation of Ag-AgVO₃/g-C₃N₄ composite photo-catalyst and degradation characteristics of antibiotics. *J. Hazard. Mater.* **2019**, *373*, 303–312. [[CrossRef](#)] [[PubMed](#)]
23. Guo, Y.; Li, M.; Huang, X.; Wu, Y.; Li, L. S-scheme g-C₃N₄/TiO₂/CFs heterojunction composites with multi-dimensional through-holes and enhanced visible-light photocatalytic activity. *Ceram. Int.* **2022**, *48*, 8196–8208. [[CrossRef](#)]
24. Kumar, A.; Kumar, A.; Sharma, G.; Al-Muhtaseb, A.H.; Naushad, M.; Ghfar, A.A.; Stadler, F.J. Quaternary magnetic BiOCl/g-C₃N₄/Cu₂O/Fe₃O₄ nano-junction for visible light and solar powered degradation of sulfamethoxazole from aqueous environment. *Chem. Eng. J.* **2018**, *334*, 462–478. [[CrossRef](#)]
25. Wang, S.; Liu, Y.; Wang, J. Peroxymonosulfate activation by Fe–Co–O-Codoped graphite carbon nitride for degradation of sulfamethoxazole. *Environ. Sci. Technol.* **2020**, *54*, 10361–10369. [[CrossRef](#)] [[PubMed](#)]
26. Liang, J.; Zhang, W.; Zhao, Z.; Liu, W.; Ye, J.; Tong, M.; Li, Y. Different degradation mechanisms of carbamazepine and diclofenac by single-atom Barium embedded g-C₃N₄: The role of photosensitization-like mechanism. *J. Hazard. Mater.* **2021**, *416*, 125936. [[CrossRef](#)]
27. Tian, Y.; Tian, X.; Zeng, W.; Nie, Y.; Yang, C.; Dai, C.; Li, Y.; Lu, L. Enhanced peroxymonosulfate decomposition into ·OH and ¹O₂ for sulfamethoxazole degradation over Se doped g-C₃N₄ due to induced exfoliation and N vacancies formation. *Sep. Purif. Technol.* **2021**, *267*, 118664. [[CrossRef](#)]
28. Xu, Q.; Zhang, L.; Cheng, B.; Fan, J.; Yu, J. S-scheme heterojunction photocatalyst. *Chem* **2020**, *6*, 1543–1559. [[CrossRef](#)]
29. Tada, H.; Mitsui, T.; Kiyonaga, T.; Akita, T.; Tanaka, K. All solid-state Z-scheme in Cds-Au-TiO₂ three component nanojunction system. *Nat. Mater.* **2006**, *5*, 782–786. [[CrossRef](#)]
30. Chen, W.; He, Z.; Huang, G.; Wu, C.; Chen, W.; Liu, X. Direct Z scheme 2D/2D MnIn₂S₄/g-C₃N₄ architectures with highly efficient photocatalytic activities towards treatment of pharmaceutical wastewater and hydrogen evolution. *Chem. Eng. J.* **2019**, *359*, 244–253. [[CrossRef](#)]
31. Pham, V.V.; Truong, T.K.; Hai, L.V.; La, H.P.P.; Nguyen, H.T.; Lam, V.Q.; Tong, H.D.; Nguyen, T.Q.; Sabbah, A.; Chen, K.; et al. S-Scheme α-Fe₂O₃/g-C₃N₄ nanocomposites as heterojunction photocatalysts for antibiotic degradation. *Appl. Nanomater.* **2022**, *5*, 4506–4514. [[CrossRef](#)]
32. Ni, S.; Fu, Z.; Li, L.; Ma, M.; Liu, Y. Step-scheme heterojunction g-C₃N₄/TiO₂ for efficient photocatalytic degradation of tetracycline hydrochloride under UV light. *Colloids Surf. A Physicochem. Eng. Asp.* **2022**, *649*, 129475. [[CrossRef](#)]
33. Zhang, Q.; Peng, Y.; Deng, F.; Wang, M.; Chen, D. Porous Z-scheme MnO₂/Mn-modified alkalized g-C₃N₄ heterojunction with excellent Fenton-like photocatalytic activity for efficient degradation of pharmaceutical pollutants. *Sep. Purif. Technol.* **2020**, *246*, 116890. [[CrossRef](#)]
34. Mei, X.; Chen, S.; Wang, G.; Chen, W.; Lu, W.; Zhang, B.; Fang, Y.; Qi, C. Metal-free carboxyl modified g-C₃N₄ for enhancing photocatalytic degradation activity of organic pollutants through peroxymonosulfate activation in wastewater under solar irradiation. *J. Solid State Chem.* **2022**, *310*, 123053. [[CrossRef](#)]
35. Luo, J.; Dai, Y.; Xu, X.; Liu, Y.; Yang, S.; He, H.; Sun, C.; Xia, Q. Green and efficient synthesis of Co-MOF-based/g-C₃N₄ composite catalysts to activate peroxymonosulfate for degradation of the antidepressant venlafaxine. *J. Colloid Interf. Sci.* **2022**, *610*, 280–294. [[CrossRef](#)] [[PubMed](#)]
36. Wang, S.; Wang, J. Magnetic 2D/2D oxygen doped g-C₃N₄/biochar composite to activate peroxymonosulfate for degradation of emerging organic pollutants. *J. Hazard. Mater.* **2022**, *423*, 127207. [[CrossRef](#)] [[PubMed](#)]
37. Liu, C.; Dai, H.; Tan, C.; Pan, Q.; Hu, F.; Peng, X. Photo-Fenton degradation of tetracycline over Z-scheme Fe-g-C₃N₄/Bi₂WO₆ heterojunctions: Mechanism insight, degradation pathways and DFT calculation. *Appl. Catal. B Environ.* **2022**, *310*, 121326. [[CrossRef](#)]
38. Li, T.; Ge, L.; Peng, X.; Wang, W.; Zhang, W. Enhanced degradation of sulfamethoxazole by a novel Fenton-like system with significantly reduced consumption of H₂O₂ activated by g-C₃N₄/MgO composite. *Water Res.* **2021**, *190*, 116777. [[CrossRef](#)]
39. Li, X.; Gan, X. Photo-Fenton degradation of multiple pharmaceuticals at low concentrations via Cu-doped-graphitic carbon nitride (g-C₃N₄) under simulated solar irradiation at a wide pH range. *J. Environ. Chem. Eng.* **2022**, *10*, 108290. [[CrossRef](#)]
40. Cao, Z.; Jia, Y.; Wang, Q.; Cheng, H. High-efficiency photo-Fenton Fe/g-C₃N₄/kaolinite catalyst for tetracycline hydrochloride degradation. *Appl. Clay Sci.* **2021**, *212*, 106213. [[CrossRef](#)]
41. Qiao, X.; Liu, X.; Zhang, W.; Cai, Y.; Zhong, Z.; Li, Y.; Lu, J. Superior photo-Fenton activity towards chlortetracycline degradation over novel g-C₃N₄ nanosheets/schwertmannite nanocomposites with accelerated Fe(III)/Fe(II) cycling. *Sep. Purif. Technol.* **2021**, *279*, 119760. [[CrossRef](#)]
42. Zhang, J.; Zhao, Y.; Zhang, K.; Zada, A.; Qi, K. Sonocatalytic degradation of tetracycline hydrochloride with CoFe₂O₄/g-C₃N₄ composite. *Ultrason. Sonochem.* **2023**, *94*, 106325. [[CrossRef](#)]
43. He, Y.; Ma, Z.; Junior, L.B. Distinctive binary g-C₃N₄/MoS₂ heterojunctions with highly efficient ultrasonic catalytic degradation for levofloxacin and methylene blue. *Ceram. Int.* **2020**, *46*, 12364–12372. [[CrossRef](#)]
44. Vinesh, V.; Ashokkumar, M.; Neppolian, B. rGO supported self-assembly of 2D nano sheet of (g-C₃N₄) into rod-like nano structure and its application in sonophotocatalytic degradation of an antibiotic. *Ultrason. Sonochem.* **2020**, *68*, 105218. [[CrossRef](#)]

45. Gholami, P.; Khataee, A.; Vahid, B.; Karimi, A.; Golizadeh, M.; Ritala, M. Sonophotocatalytic degradation of sulfadiazine by integration of microfibrillated carboxymethyl cellulose with Zn-Cu-Mg mixed metal hydroxide/g-C₃N₄ composite. *Sep. Purif. Technol.* **2020**, *245*, 116866. [[CrossRef](#)]
46. Jiang, L.; Yuan, X.; Zeng, G.; Liang, J.; Wu, Z.; Yu, H.; Mo, D.; Wang, H.; Xiao, Z.; Zhou, C. Nitrogen self-doped g-C₃N₄ nanosheets with tunable band structures for enhanced photocatalytic tetracycline degradation. *J. Colloid Interf. Sci.* **2019**, *536*, 17–29. [[CrossRef](#)]
47. Palanivel, B.; Shkir, M.; Alshahrani, T.; Mani, A. Novel NiFe₂O₄ deposited S-doped g-C₃N₄ nanorod: Visible-light-driven heterojunction for photo-Fenton like tetracycline degradation. *Diam. Relat. Mater.* **2021**, *112*, 108148. [[CrossRef](#)]
48. Preeyanga, M.; Dhileepan, M.D.; Madhavan, J.; Neppolian, B. Revealing the charge transfer mechanism in magnetically recyclable ternary g-C₃N₄/BiOBr/Fe₃O₄ nanocomposite for efficient photocatalytic degradation of tetracycline antibiotics. *Chemosphere* **2022**, *303*, 135070. [[CrossRef](#)]
49. Bui, T.S.; Bansal, P.; Lee, B.; Mahvelati-Shamsabadi, T. Facile fabrication of novel Ba-doped g-C₃N₄ photocatalyst with remarkably enhanced photocatalytic activity towards tetracycline elimination under visible-light irradiation. *Appl. Surf. Sci.* **2020**, *506*, 144184. [[CrossRef](#)]
50. Cao, Y.; Alsharif, S.; El-Shafay, A.S. Preparation, suppressed the charge carriers recombination, and improved photocatalytic performance of g-C₃N₄/MoS₂ p-n heterojunction photocatalyst for tetracycline and dyes degradation upon visible light. *Mater. Sci. Semicond. Process.* **2022**, *144*, 106569. [[CrossRef](#)]
51. Cao, Z.; Zhao, Y.; Li, J.; Wang, Q.; Mei, Q.; Cheng, H. Rapid electron transfer-promoted tetracycline hydrochloride degradation: Enhanced activity in visible light-coupled peroxymonosulfate with PdO/g-C₃N₄/kaolinite catalyst. *Chem. Eng. J.* **2023**, *457*, 141191. [[CrossRef](#)]
52. Chen, H.; Zhang, X.; Jiang, L.; Yuan, X.; Liang, J.; Zhang, J.; Yu, H.; Chu, W.; Wu, Z.; Li, H.; et al. Strategic combination of nitrogen-doped carbon quantum dots and g-C₃N₄: Efficient photocatalytic peroxydisulfate for the degradation of tetracycline hydrochloride and mechanism insight. *Sep. Purif. Technol.* **2021**, *272*, 118947. [[CrossRef](#)]
53. Guo, F.; Shi, W.; Wang, H.; Han, M.; Li, H.; Huang, H.; Liu, Y.; Kang, Z. Facile fabrication of a CoO/g-C₃N₄ p-n heterojunction with enhanced photocatalytic activity and stability for tetracycline degradation under visible light. *Catal. Sci. Technol.* **2017**, *7*, 3325–3331. [[CrossRef](#)]
54. Guo, F.; Shi, W.; Li, M.; Shi, Y.; Wen, H. 2D/2D Z-scheme heterojunction of CuInS₂/g-C₃N₄ for enhanced visible-light-driven photocatalytic activity towards the degradation of tetracycline. *Sep. Purif. Technol.* **2019**, *210*, 608–615. [[CrossRef](#)]
55. Guo, F.; Huang, X.; Chen, Z.; Sun, H.; Chen, L. Prominent co-catalytic effect of CoP nanoparticles anchored on high-crystalline g-C₃N₄ nanosheets for enhanced visible-light photocatalytic degradation of tetracycline in wastewater. *Chem. Eng. J.* **2020**, *395*, 125118. [[CrossRef](#)]
56. Guo, B.; Liu, B.; Wang, C.; Lu, J.; Wang, Y.; Yin, S.; Javed, M.S.; Han, W. Boosting photocharge separation in Z-schemed g-C₃N₄/RGO/In₂S₃ photocatalyst for H₂ evolution and antibiotic degradation. *J. Ind. Eng. Chem.* **2022**, *110*, 217–224. [[CrossRef](#)]
57. He, Y.; Ma, B.; Yang, Q.; Tong, Y.; Ma, Z.; Junior, L.B.; Yao, B. Surface construction of a novel metal-free g-C₃N₄-based heterojunction photocatalyst for the efficient removal of bio-toxic antibiotic residues. *Appl. Surf. Sci.* **2022**, *571*, 151299. [[CrossRef](#)]
58. Huang, H.; Liu, C.; Ou, H.; Ma, T.; Zhang, Y. Self-sacrifice transformation for fabrication of type-I and type-II heterojunctions in hierarchical Bi_xO_yI_z/g-C₃N₄ for efficient visible-light photocatalysis. *Appl. Surf. Sci.* **2019**, *470*, 1101–1110. [[CrossRef](#)]
59. Obregon, S.; Ruiz-Gomez, M.A.; Rodriguez-Gonzalez, V.; Vaquez, A.; Hernandez-Uresti, D.B. A novel type-II Bi₂W₂O₉/g-C₃N₄ heterojunction with enhanced photocatalytic performance under simulated solar irradiation. *Mater. Sci. Semicond. Process.* **2020**, *113*, 105056. [[CrossRef](#)]
60. Panneri, S.; Ganguly, P.; Mohan, M.; Nair, B.N.; Mohamed, A.A.P.; Warriar, K.G.; Hareesh, U.S. Photoregenerable, bifunctional granules of carbon-doped g-C₃N₄ as adsorptive photocatalyst for the efficient removal of tetracycline antibiotic. *ACS Sustain. Chem. Eng.* **2017**, *5*, 1610–1618. [[CrossRef](#)]
61. Peng, X.; Wu, J.; Zhao, Z.; Wang, X.; Dai, H.; Xu, L.; Xu, G.; Jian, Y.; Hu, F. Activation of peroxymonosulfate by single-atom Fe-g-C₃N₄ catalysts for high efficiency degradation of tetracycline via nonradical pathways: Role of high-valent iron-oxo species and Fe-N_x sites. *Chem. Eng. J.* **2022**, *427*, 130803. [[CrossRef](#)]
62. Ren, Z.; Chen, F.; Wen, K.; Lu, J. Enhanced photocatalytic activity for tetracyclines degradation with Ag modified g-C₃N₄ composite under visible light. *J. Photochem. Photobiol. A Chem.* **2020**, *389*, 112217. [[CrossRef](#)]
63. Ren, X.; Zhang, X.; Guo, R.; Li, X.; Peng, Y.; Zhao, X.; Pu, X. Hollow mesoporous g-C₃N₄/Ag₂CrO₄ photocatalysis with direct Z-scheme: Excellent degradation performance for antibiotics and dyes. *Sep. Purif. Technol.* **2021**, *270*, 118797. [[CrossRef](#)]
64. Shi, Y.; Li, J.; Sun, Y.; Wan, D.; Wan, H.; Wang, Y. FeOOH coupling and nitrogen vacancies functionalized g-C₃N₄ heterojunction for efficient degradation of antibiotics: Performance evaluation, active species evolution and mechanism insight. *J. Alloy. Compd.* **2022**, *903*, 163898. [[CrossRef](#)]
65. Song, H.; Liu, L.; Wang, H.; Feng, B.; Xiao, M.; Tang, Y.; Qu, X.; Gai, H.; Huang, T. Adjustment of the band gap of co-doped KCl/NH₄Cl/g-C₃N₄ for enhanced photocatalytic performance under visible light. *Mater. Sci. Semicond. Process.* **2021**, *128*, 105757. [[CrossRef](#)]
66. Tian, Y.; Gao, Y.; Wang, Q.; Wang, Z.; Guan, R.; Shi, W. Potassium gluconate-cooperative pore generation based on g-C₃N₄ nanosheets for highly efficient photocatalytic hydrogen production and antibiotic degradation. *J. Environ. Chem. Eng.* **2022**, *10*, 107986. [[CrossRef](#)]

67. Wang, W.; Zeng, Z.; Zeng, G.; Zhang, C.; Xiao, R.; Zhou, C.; Xiong, W.; Yang, Y.; Lei, L.; Liu, Y.; et al. Sulfur doped carbon quantum dots loaded hollow tubular g-C₃N₄ as novel photocatalyst for destruction of *Escherichia coli* and tetracycline degradation under visible light. *Chem. Eng. J.* **2019**, *378*, 122132. [CrossRef]
68. Wang, W.; Fang, J.; Chen, H. Nano-confined g-C₃N₄ in mesoporous SiO₂ with improved quantum size effect and tunable structure for photocatalytic tetracycline antibiotic degradation. *J. Alloy. Compd.* **2020**, *819*, 153064. [CrossRef]
69. Wang, Q.; Zhang, L.; Guo, Y.; Shen, M.; Wang, M.; Li, B.; Shi, J. Multifunctional 2D porous g-C₃N₄ nanosheets hybridized with 3D hierarchical TiO₂ microflowers for selective dye adsorption, antibiotic degradation and CO₂ reduction. *Chem. Eng. J.* **2020**, *396*, 125347. [CrossRef]
70. Wang, M.; Jin, C.; Kang, J.; Liu, J.; Tang, Y.; Li, Z.; Li, S. CuO/g-C₃N₄ 2D/2D heterojunction photocatalysts as efficient peroxymonosulfate activators under visible light for oxytetracycline degradation: Characterization, efficiency and mechanism. *Chem. Eng. J.* **2021**, *416*, 128118. [CrossRef]
71. Wu, K.; Chen, D.; Fang, J.; Wu, S.; Yang, F.; Zhu, X.; Fang, Z. One-step synthesis of sulfur and tungstate co-doped porous g-C₃N₄ microrods with remarkably enhanced visible-light photocatalytic performances. *Appl. Surf. Sci.* **2018**, *462*, 991–1001. [CrossRef]
72. Wu, K.; Chen, D.; Lu, S.; Fang, J.; Zhu, X.; Yang, F.; Pan, T.; Fang, Z. Supramolecular self-assembly synthesis of noble-metal-free (C, Ce) co-doped g-C₃N₄ with porous structure for highly efficient photocatalytic degradation of organic pollutants. *J. Hazard. Mater.* **2020**, *382*, 121027. [CrossRef] [PubMed]
73. Wu, C.; Zuo, H.; Du, H.; Zhang, S.; Wang, L.; Yan, Q. Construction of layered embedding dual Z-Scheme Bi₂O₂CO₃/g-C₃N₄/Bi₂O₃: Tetracycline degradation pathway, toxicity analysis and mechanism insight. *Sep. Purif. Technol.* **2022**, *282*, 120096. [CrossRef]
74. Xu, Y.; Ge, F.; Chen, Z.; Huang, S.; Wei, W.; Xie, M.; Xu, H.; Li, H. One-step synthesis of Fe-doped surface-alkalinized g-C₃N₄ and their improved visible-light photocatalytic performance. *Appl. Surf. Sci.* **2019**, *469*, 739–746. [CrossRef]
75. Zhang, C.; Ouyang, Z.; Yang, Y.; Long, X.; Qin, L.; Wang, W.; Zhou, Y.; Qin, D.; Qin, F.; Lai, C. Molecular engineering of donor-acceptor structured g-C₃N₄ for superior photocatalytic oxytetracycline degradation. *Chem. Eng. J.* **2022**, *448*, 137370. [CrossRef]
76. Zhao, C.; Ran, F.; Dai, L.; Li, C.; Zheng, C.; Si, C. Cellulose-assisted construction of high surface area Z-scheme C-doped g-C₃N₄/WO₃ for improved tetracycline degradation. *Carbohydr. Polym.* **2021**, *255*, 117343. [CrossRef]
77. Lu, C.; Wang, J.; Cao, D.; Guo, F.; Hao, X.; Li, D.; Shi, W. Synthesis of magnetically recyclable g-C₃N₄/NiFe₂O₄ S-scheme heterojunction photocatalyst with promoted visible-light-response photo-Fenton degradation of tetracycline. *Mater. Res. Bull.* **2023**, *158*, 112064. [CrossRef]
78. Li, F.; Huang, T.; Sun, F.; Chen, L.; Li, P.; Shao, F.; Yang, X.; Liu, W. Ferric oxide nanoclusters with low-spin Fe^{III} anchored g-C₃N₄ rod for boosting photocatalytic activity and degradation of diclofenac in water under solar light. *Appl. Catal. B Environ.* **2022**, *317*, 121725. [CrossRef]
79. Papamichail, P.; Nannou, C.; Giannakoudakis, D.A.; Bikiaris, N.D.; Papoulia, C.; Pavlidou, E.; Lambropoulou, D.; Samanidou, V.; Deliyanni, E. Maximization of the photocatalytic degradation of diclofenac using polymeric g-C₃N₄ by tuning the precursor and the synthetic protocol. *Catal. Today* **2023**, *418*, 114075. [CrossRef]
80. Jin, X.; Wu, Y.; Wang, Y.; Lin, Z.; Liang, D.; Zheng, X.; Wei, D.; Liu, H.; Lv, W.; Liu, G. Carbon quantum dots-modified reduced ultrathin g-C₃N₄ with strong photoredox capacity for broad spectrum-driven PPCPs remediation in natural water matrices. *Chem. Eng. J.* **2021**, *420*, 129935. [CrossRef]
81. Hu, Z.; Cai, X.; Wang, Z.; Li, S.; Wang, Z.; Xie, X. Construction of carbon-doped supramolecule-based g-C₃N₄/TiO₂ composites for removal of diclofenac and carbamazepine: A comparative study of operating parameters, mechanisms, degradation pathways. *J. Hazard. Mater.* **2019**, *380*, 120812. [CrossRef] [PubMed]
82. John, P.; Johari, K.; Gnanasundaram, N.; Appusamy, A.; Thanabalan, M. Enhanced photocatalytic performance of visible light driven TiO₂/g-C₃N₄ for degradation of diclofenac in aqueous solution. *Environ. Technol. Innov.* **2021**, *22*, 101412. [CrossRef]
83. Han, Y.; Gan, L.; Gong, H.; Han, J.; Qiao, W.; Xu, L. Photoactivation of peroxymonosulfate by wood pulp cellulose biochar/g-C₃N₄ composite for diclofenac degradation: The radical and nonradical pathways. *Biochar* **2022**, *4*, 35. [CrossRef]
84. Jimenez-Salcedo, M.; Monge, M.; Tena, M.T. The photocatalytic degradation of sodium diclofenac in different water matrices using g-C₃N₄ nanosheets: A study of the intermediate by-products and mechanism. *J. Environ. Chem. Eng.* **2021**, *9*, 105827. [CrossRef]
85. Oliveros, A.N.; Pimentel, J.A.I.; Luna, M.D.G.; Garcia-Segura, S.; Abarca, R.R.M.; Doong, R. Visible-light photocatalytic diclofenac removal by tunable vanadium pentoxide/boron-doped graphitic carbon nitride composite. *Chem. Eng. J.* **2021**, *403*, 126213. [CrossRef]
86. Muelas-Ramos, V.; Sampaio, M.J.; Silva, C.G.; Bedia, J.; Rodriguez, J.J.; Faria, J.L. Degradation of diclofenac in water under LED irradiation using combined g-C₃N₄/NH₂-MIL-125 photocatalysts. *J. Hazard. Mater.* **2021**, *416*, 126199. [CrossRef]
87. Reddy, C.V.; Kakarla, R.R.; Cheolho, B.; Shim, J.; Aminabhavi, T.M. Heterostructured 2D/2D ZnIn₂S₄/g-C₃N₄ nanohybrids for photocatalytic degradation of antibiotic sulfamethoxazole and photoelectrochemical properties. *Environ. Res.* **2023**, *225*, 115585. [CrossRef] [PubMed]
88. Peng, W.; Liao, J.; Chen, L.; Wu, X.; Zhang, X.; Sun, W.; Ge, C. Constructing a 3D interconnected “trap-zap” β-CDPs/Fe-g-C₃N₄ catalyst for efficient sulfamethoxazole degradation via peroxymonosulfate activation: Performance, mechanism, intermediates and toxicity. *Chemosphere* **2022**, *294*, 133780. [CrossRef]

89. Li, Y.; Li, J.; Pan, Y.; Xiong, Z.; Yao, G.; Xie, R.; Lai, B. Peroxymonosulfate activation on FeCo₂S₄ modified g-C₃N₄ (FeCo₂S₄-CN): Mechanism of singlet oxygen evolution for nonradical efficient degradation of sulfamethoxazole. *Chem. Eng. J.* **2020**, *384*, 123361. [[CrossRef](#)]
90. Zhao, G.; Li, W.; Zhang, H.; Wang, W.; Ren, Y. Single atom Fe-dispersed graphitic carbon nitride (g-C₃N₄) as a highly efficient peroxymonosulfate photocatalytic activator for sulfamethoxazole degradation. *Chem. Eng. J.* **2022**, *430*, 132937. [[CrossRef](#)]
91. Zhou, L.; Zhang, W.; Chen, L.; Deng, H.; Wan, J. A novel ternary visible-light-driven photocatalyst AgCl/Ag₃PO₄/g-C₃N₄: Synthesis, characterization, photocatalytic activity for antibiotic degradation and mechanism analysis. *Catal. Commun.* **2017**, *100*, 191–195. [[CrossRef](#)]
92. Liu, G.; Zhang, Z.; Lv, M.; Wang, H.; Chen, D.; Feng, Y. Photodegradation performance and transformation mechanisms of sulfamethoxazole by porous g-C₃N₄ modified with ammonia bicarbonate. *Sep. Purif. Technol.* **2020**, *235*, 116172. [[CrossRef](#)]
93. Zhou, L.; Zhang, W.; Chen, L.; Deng, H. Z-scheme mechanism of photogenerated carriers for hybrid photocatalyst Ag₃PO₄/g-C₃N₄ in degradation of sulfamethoxazole. *J. Colloid Interface Sci.* **2017**, *487*, 410–417. [[CrossRef](#)] [[PubMed](#)]
94. Song, Y.; Qi, J.; Tian, J.; Gao, S.; Cui, F. Construction of Ag/g-C₃N₄ photocatalysts with visible-light photocatalytic activity for sulfamethoxazole degradation. *Chem. Eng. J.* **2018**, *341*, 547–555. [[CrossRef](#)]
95. Zhang, H.; Li, W.; Yan, Y.; Wang, W.; Ren, Y.; Li, X. Synthesis of highly porous g-C₃N₄ nanotubes for efficient photocatalytic degradation of sulfamethoxazole. *Mater. Today Commun.* **2021**, *27*, 102288. [[CrossRef](#)]
96. Liang, H.; Guo, J.; Yu, M.; Zhou, Y.; Zhan, R.; Liu, C.; Niu, J. Porous loofah-sponge-like ternary heterojunction g-C₃N₄/Bi₂WO₆/MoS₂ for highly efficient photocatalytic degradation of sulfamethoxazole under visible light irradiation. *Chemosphere* **2021**, *279*, 130552. [[CrossRef](#)]
97. Liu, S.; Tang, W. Photodecomposition of ibuprofen over g-C₃N₄/Bi₂WO₆/rGO heterostructured composites under visible/solar light. *Sci. Total Environ.* **2020**, *731*, 139172. [[CrossRef](#)]
98. Mao, S.; Liu, C.; Xia, M.; Wang, F.; Ju, X. Construction of a Z-scheme 1D/2D FeV₃O₈/g-C₃N₄ composite for ibuprofen degradation: Mechanism insight, theoretical calculation and degradation pathway. *Catal. Sci. Technol.* **2021**, *11*, 3466–3480. [[CrossRef](#)]
99. Meng, F.; Wang, J.; Tian, W.; Zhang, H.; Liu, S.; Tan, X.; Wang, S. Effects of inter/intralayer adsorption and direct/indirect reaction on photo-removal of pollutants by layered g-C₃N₄ and BiOBr. *J. Clean. Prod.* **2021**, *322*, 129025. [[CrossRef](#)]
100. Akbarzadeh, R.; Fung, C.S.L.; Rather, R.A.; Lo, I.M.C. One-pot hydrothermal synthesis of g-C₃N₄/Ag/AgCl/BiVO₄ micro-flower composite for the visible light degradation of ibuprofen. *Chem. Eng. J.* **2018**, *341*, 248–261. [[CrossRef](#)]
101. Cao, W.; Yuan, Y.; Yang, C.; Wu, S.; Cheng, J. In-situ fabrication of g-C₃N₄/MIL-68(In)-NH₂ heterojunction composites with enhanced visible-light photocatalytic activity for degradation of ibuprofen. *Chem. Eng. J.* **2020**, *391*, 123608. [[CrossRef](#)]
102. Chen, X.; Li, X.; Yang, J.; Sun, Q.; Yang, Y.; Wu, X. Multiphase TiO₂ surface coating g-C₃N₄ formed a sea urchin like structure with interface effects and improved visible-light photocatalytic performance for the degradation of ibuprofen. *Int. J. Hydrog. Energy* **2018**, *43*, 13284–13293. [[CrossRef](#)]
103. Jimenez-Salcedo, M.; Monge, M.; Tena, M.T. Photocatalytic degradation of ibuprofen in water using TiO₂/UV and g-C₃N₄/visible light: Study of intermediate degradation products by liquid chromatography coupled to high-resolution mass spectrometry. *Chemosphere* **2019**, *215*, 605–618. [[CrossRef](#)] [[PubMed](#)]
104. Jimenez-Salcedo, M.; Monge, M.; Tena, M.T. Combination of Au-Ag plasmonic nanoparticles of varied compositions with carbon nitride for enhanced photocatalytic degradation of Ibuprofen under visible light. *Materials* **2021**, *14*, 3912. [[CrossRef](#)]
105. Liang, M.; Zhang, Z.; Long, R.; Wang, Y.; Yu, Y.; Pei, Y. Design of a Z-scheme g-C₃N₄/CQDs/CdIn₂S₄ composite for efficient visible-light-driven photocatalytic degradation of ibuprofen. *Environ. Pollut.* **2020**, *259*, 113770. [[CrossRef](#)]
106. Liu, R.; Sun, L.; Qiao, Y.; Bie, Y.; Wang, P.; Zhang, X.; Zhang, Q. Efficient photocatalytic degradation of pharmaceutical pollutants using plasma-treated g-C₃N₄/TiO₂. *Energy Technol.* **2020**, *8*, 2000095. [[CrossRef](#)]
107. Liu, S.; Tang, W.; Chou, P. Microwave-assisted synthesis of triple 2D g-C₃N₄/Bi₂WO₆/rGO composites for ibuprofen photodegradation: Kinetics, mechanism and toxicity evaluation of degradation products. *Chem. Eng. J.* **2020**, *387*, 124098. [[CrossRef](#)]
108. Wang, J.; Tang, L.; Zeng, G.; Deng, Y.; Liu, Y.; Wang, L.; Zhou, Y.; Guo, Z.; Wang, J.; Zhang, C. Atomic scale g-C₃N₄/Bi₂WO₆ 2D/2D heterojunction with enhanced photocatalytic degradation of ibuprofen under visible light irradiation. *Appl. Catal. B Environ.* **2017**, *209*, 285–294. [[CrossRef](#)]
109. Wei, Q.; Xiong, S.; Li, W.; Jin, C.; Chen, Y.; Hou, L.; Wu, Z.; Pan, Z.; He, Q.; Wang, Y.; et al. Double Z-scheme system of α-SnWO₄/UiO-66(NH₂)/g-C₃N₄ ternary heterojunction with enhanced photocatalytic performance for ibuprofen degradation and H₂ evolution. *J. Alloy. Compd.* **2021**, *885*, 160984. [[CrossRef](#)]
110. Deng, Y.; Tang, L.; Feng, C.; Zeng, G.; Wang, J.; Zhou, Y.; Liu, Y.; Peng, B.; Feng, H. Construction of plasmonic Ag modified phosphorous-doped ultrathin g-C₃N₄ nanosheets/BiVO₄ photocatalyst with enhanced visible-near-infrared response ability for ciprofloxacin degradation. *J. Hazard. Mater.* **2018**, *344*, 758–769. [[CrossRef](#)]
111. Zhang, N.; Li, X.; Wang, Y.; Zhu, B.; Yang, J. Fabrication of magnetically recoverable Fe₃O₄/CdS/g-C₃N₄ photocatalysts for effective degradation of ciprofloxacin under visible light. *Ceram. Int.* **2020**, *46*, 20974–20984. [[CrossRef](#)]
112. Savunthari, K.V.; Arunagiri, D.; Shanmugam, S.; Ganesan, S.; Arasu, M.V.; Al-Dhabi, N.A.; Chi, N.T.L.; Ponnusamy, V.K. Green synthesis of lignin nanorods/g-C₃N₄ nanocomposite materials for efficient photocatalytic degradation of triclosan in environmental water. *Chemosphere* **2021**, *272*, 129801. [[CrossRef](#)] [[PubMed](#)]
113. Wang, J.; Yue, M.; Han, Y.; Xu, X.; Yue, Q.; Xu, S. Highly-efficient degradation of triclosan attributed to peroxymonosulfate activation by heterogeneous catalyst g-C₃N₄/MnFe₂O. *Chem. Eng. J.* **2020**, *391*, 123554. [[CrossRef](#)]

114. Yu, B.; Yan, W.; Meng, Y.; Zhang, Y.; Li, X.; Zhong, Y.; Ding, J.; Zhang, H. Selected dechlorination of triclosan by high-performance g-C₃N₄/Bi₂MoO₆ composites: Mechanisms and pathways. *Chemosphere* **2023**, *312*, 137247. [CrossRef]
115. Mafa, P.J.; Malfane, M.E.; Idris, A.O.; Liu, D.; Gui, J.; Mamba, B.B.; Kuvarega, A.T. Multi-elemental doped g-C₃N₄ with enhanced visible light photocatalytic Activity: Insight into naproxen Degradation, Kinetics, effect of Electrolytes, and mechanism. *Sep. Purif. Technol.* **2022**, *282*, 120089. [CrossRef]
116. Truong, H.B.; Huy, B.T.; Ray, S.K.; Gyawali, G.; Lee, Y.; Cho, J.; Hur, J. Magnetic visible-light activated photocatalyst ZnFe₂O₄/BiVO₄/g-C₃N₄ for decomposition of antibiotic lomefloxacin: Photocatalytic mechanism, degradation pathway, and toxicity assessment. *Chemosphere* **2022**, *299*, 134320. [CrossRef]
117. Mirzaei, A.; Chen, Z.; Haghghat, F.; Yerushalmi, L. Magnetic fluorinated mesoporous g-C₃N₄ for photocatalytic degradation of amoxicillin: Transformation mechanism and toxicity assessment. *Appl. Catal. B Environ.* **2019**, *242*, 337–348. [CrossRef]
118. Saravanakumar, K.; Park, C.M. Rational design of a novel LaFeO₃/g-C₃N₄/BiFeO₃ double Z-scheme structure: Photocatalytic performance for antibiotic degradation and mechanistic insight. *Chem. Eng. J.* **2021**, *423*, 130076. [CrossRef]
119. Xie, X.; Chen, C.; Wang, X.; Li, J.; Naraginti, S. Efficient detoxification of triclosan by a S-Ag/TiO₂@g-C₃N₄ hybrid photocatalyst: Process optimization and bio-toxicity assessment. *RSC Adv.* **2019**, *9*, 20439–20449. [CrossRef]
120. Su, Q.; Li, J.; Yuan, H.; Wang, B.; Wang, Y.; Li, Y.; Xing, Y. Visible-light-driven photocatalytic degradation of ofloxacin by g-C₃N₄/NH₂-MIL-88B(Fe) heterostructure: Mechanisms, DFT calculation, degradation pathway and toxicity evolution. *Chem. Eng. J.* **2022**, *427*, 131594. [CrossRef]
121. Huang, D.; Sun, X.; Liu, Y.; Ji, H.; Liu, W.; Wang, C.; Ma, W.; Cai, Z. A carbon-rich g-C₃N₄ with promoted charge separation for highly efficient photocatalytic degradation of amoxicillin. *Chin. Chem. Lett.* **2021**, *32*, 2787–2791. [CrossRef]
122. Nivetha, M.S.; Kumar, J.V.; Ajarem, J.S.; Allam, A.A.; Manikandan, V.; Arulmozhi, R.; Abirami, N. Construction of SnO₂/g-C₃N₄ an effective nanocomposite for photocatalytic degradation of amoxicillin and pharmaceutical effluent. *Environ. Res.* **2022**, *209*, 112809. [CrossRef] [PubMed]
123. Dai, S.; Xiao, L.; Li, Q.; Hao, G.; Hu, Y.; Jiang, W. 0D/1D Co₃O₄ quantum dots/surface hydroxylated g-C₃N₄ nanofibers heterojunction with enhanced photocatalytic removal of pharmaceuticals and personal care products. *Sep. Purif. Technol.* **2022**, *297*, 121481. [CrossRef]
124. Thang, N.Q.; Sabbah, A.; Chen, L.; Chen, K.; Thi, C.M.; Viet, P.V. High-efficient photocatalytic degradation of commercial drugs for pharmaceutical wastewater treatment prospects: A case study of Ag/g-C₃N₄/ZnO nanocomposite materials. *Chemosphere* **2021**, *282*, 130971. [CrossRef] [PubMed]
125. Liu, Z.; Zhang, A.; Liu, Y.; Fu, Y.; Du, Y. Local surface plasmon resonance (LSPR)-coupled charge separation over g-C₃N₄-supported WO₃/BiOCl heterojunction for photocatalytic degradation of antibiotics. *Colloids Surf. A Physicochem. Eng. Asp.* **2022**, *643*, 128818. [CrossRef]
126. Shanavas, S.; Roopan, S.M.; Priyadharshan, A.; Devipriya, D.; Jayapandi, S.; Acevedo, R.; Anbarasan, P.M. Computationally guided synthesis of (2D/3D/2D) rGO/Fe₂O₃/g-C₃N₄ nanostructure with improved charge separation and transportation efficiency for degradation of pharmaceutical molecules. *Appl. Catal. B Environ.* **2019**, *255*, 117758. [CrossRef]
127. Qarajehdaghi, M.; Mehrizad, A.; Gharbani, P.; Shahverdzadeh, G.H. Quaternary composite of CdS/g-C₃N₄/rGO/CMC as a susceptible visible-light photocatalyst for effective abatement of ciprofloxacin: Optimization and modeling of the process by RSM and ANN. *Process Saf. Environ. Prot.* **2023**, *169*, 352–362. [CrossRef]
128. AttariKhasraghi, N.; Zare, K.; Mehrizad, A.; Modirshahla, N.; Behnajady, M.A. Zeolite 4A supported CdS/g-C₃N₄ type-II heterojunction: A novel visible-light-active ternary nanocomposite for potential photocatalytic degradation of cefoperazone. *J. Mol. Liq.* **2021**, *342*, 117479. [CrossRef]
129. Kumar, A.; Khan, M.; Zeng, X.; Lo, I.M.C. Development of g-C₃N₄/TiO₂/Fe₃O₄@SiO₂ heterojunction via sol-gel route: A magnetically recyclable direct contact Z-scheme nanophotocatalyst for enhanced photocatalytic removal of ibuprofen from real sewage effluent under visible light. *Chem. Eng. J.* **2018**, *353*, 645–656. [CrossRef]
130. Rapti, I.; Boti, V.; Albanis, T.; Konstantinou, I. Photocatalytic degradation of psychiatric pharmaceuticals in hospital WWTP secondary effluents using g-C₃N₄ and g-C₃N₄/MoS₂ catalysts in laboratory-scale pilot. *Catalysts* **2023**, *13*, 252. [CrossRef]
131. Antonopoulou, M.; Papadaki, M.; Rapti, I.; Konstantinou, I. Photocatalytic degradation of pharmaceutical amisulpride using g-C₃N₄ catalyst and UV-A irradiation. *Catalysts* **2023**, *13*, 226. [CrossRef]
132. Kumar, V.V.; Avisar, D.; Prasanna, L.V.; Betzalel, Y.; Mamane, H. Rapid visible-light degradation of EE2 and its estrogenicity in hospital wastewater by crystalline promoted g-C₃N. *J. Hazard. Mater.* **2020**, *398*, 122880.
133. Yan, W.; Yan, L.; Jing, C. Impact of doped metals on urea-derived g-C₃N₄ for photocatalytic degradation of antibiotics: Structure, photoactivity and degradation mechanisms. *Appl. Catal. B Environ.* **2019**, *244*, 475–485. [CrossRef]
134. Huang, Y.; Luo, X.; Du, Y.; Fu, Y.; Guo, X.; Zou, C.; Wu, Y. The role of iron-doped g-C₃N₄ heterogeneous catalysts in Fenton-like process investigated by experiment and theoretical simulation. *Chem. Eng. J.* **2022**, *446*, 137252. [CrossRef]
135. Hayat, A.; Al-Sehemi, A.G.; El-Nasser, K.S.; Taha, T.A.; Al-Ghamdi, A.A.; Syed, J.A.S.; Amin, M.A.; Ali, T.; Bashir, T.; Palamanit, A.; et al. Graphitic carbon nitride (g-C₃N₄)-based semiconductor as a beneficial candidate in photocatalysis diversity. *Int. J. Hydrog. Energy* **2022**, *47*, 5142–5191. [CrossRef]

136. Patnaik, S.; Sahoo, D.P.; Parida, K. Recent advances in anion doped g-C₃N₄ photocatalysts: A review. *Carbon* **2021**, *172*, 682–711. [[CrossRef](#)]
137. Yuda, A.; Kumar, A. A review of g-C₃N₄ based catalysts for direct methanol fuel cells. *Int. J. Hydrog. Energy* **2022**, *47*, 3371–3395. [[CrossRef](#)]

Disclaimer/Publisher's Note: The statements, opinions and data contained in all publications are solely those of the individual author(s) and contributor(s) and not of MDPI and/or the editor(s). MDPI and/or the editor(s) disclaim responsibility for any injury to people or property resulting from any ideas, methods, instructions or products referred to in the content.